UNIVERSIDAD DE CHILE
FACULTAD DE CIENCIAS FÍSICAS Y MATEMÁTICAS
DEPARTAMENTO DE INGENIERÍA MECÁNICA

APPLICATION OF GEOMETRY INDEPENDENT FIELD APPROXIMATION (GIFT) IN THE STUDY OF PLATE VIBRATIONS

MEMORIA PARA OPTAR AL TÍTULO DE
INGENIERO CIVIL MECÁNICO

FELIPE IGNACIO CONTRERAS ROJAS

PROFESOR GUÍA:
ELENA ATROSHCHENKO

MIEMBROS DE LA COMISIÓN:
VIVIANA MERUANE NARANJO
ALEJANDRO ORTIZ BERNARDIN

SANTIAGO DE CHILE
2018

RESUMEN DE LA MEMORIA PARA OPTAR
AL TÍTULO DE INGENIERO CIVIL MECÁNICO
POR: FELIPE IGNACIO CONTRERAS ROJAS
FECHA: 2018
PROF. GUÍA: ELENA ATROSHCHENKO

APPLICATION OF GEOMETRY INDEPENDENT FIELD APPROXIMATION (GIFT) IN THE STUDY OF PLATE VIBRATIONS

Los fenómenos físicos, presentes en las ciencias y en las diferentes áreas de la ingeniería, a menudo son modelados por Ecuaciones Diferenciales Parciales (EDP). Los problemas de valor de frontera resultantes en muchos casos carecen de soluciones analíticas. Para resolver tales problemas, uno puede hacer suposiciones que simplifiquen el problema, o usar métodos numéricos para aproximar la solución. Dentro de los métodos numéricos actualmente existentes, el más popular es el Método de Elementos Finitos (FEM), que es la base de diferentes programas comerciales, como ADINA o ANSYS, entre muchos otros. La desventaja de este método es la gran cantidad de recursos computacionales y los tiempos de iteración requeridos para obtener una solución precisa del problema.

Dada esta desventaja, Hughes desarrolló el Análisis IsoGeométrico (IGA). Este método permite integrar el modelo CAD con el Análisis de Elementos Finitos (FEA), por lo tanto, reduce los tiempos y los recursos necesarios para obtener una solución precisa. Pero a su vez, el IGA no tiene flexibilidad para obtener soluciones de ciertos problemas, ya que usa las mismas funciones bases para parametrizar tanto la geometría como el campo de solución.

Debido a esto último, surge el Análisis IsoGeométrico Generalizado (GIFT) como una generalización del IGA, este método utiliza diferentes funciones bases para parametrizar la geometría del objeto y el campo de solución, permitiendo la selección de funciones que se adapten mejor al problema estudiado. En trabajos anteriores, el GIFT ha sido aplicado a problemas de la Ecuación de Laplace y de Elasticidad Lineal.

El objetivo principal de este trabajo es estudiar el rendimiento del GIFT para problemas de flexión y de vibraciones de placas delgadas. El estudio consiste en implementar el GIFT para 3 placas diferentes y comparar los resultados numéricos con lo predicho por la Teoría de Placas de Kirchhoff-Love (KLPT). Se consideran una placa de geometría circular simple, una placa de geometría circular de dos parches y una placa cuadrada con un agujero de forma compleja, modelada por 8 parches. Las placas están parametrizadas por NURBS, mientras que las soluciones se aproximan por un parche usando NURBS o B-Splines. Los resultados se muestran en términos de curvas de convergencia, modos de vibración y frecuencias naturales.

Los resultados numéricos se comparan con las soluciones analíticas para problemas con geometría simple y con la solución FEM para el problema de una placa más compleja. El análisis realizado indica que, *para la misma parametrización de geometría (uniforme)*, (a) la solución se puede aproximar mediante un parche NURBS o B-Splines, manteniendo inalterada la geometría original, (b) los resultados obtenidos con las aproximaciones de campo NURBS y B-Splines son idénticas, (c) la tasa de convergencia depende del grado de aproximación de la solución. Para parametrizaciones geométricas no uniformes, el método no produce una tasa de convergencia óptima o resultados suficientemente precisos, al igual que el IGA tradicional.

Abstract

Physical phenomena, present in sciences and in the different areas of engineering, are often modeled by Partial Differential Equations (PDE). The resulting boundary value problems in many cases lack analytical solutions. To solve such problems, one can make assumptions that simplify the problem, or use numerical methods to approximate the solution. Within the currently existing numerical methods, the most popular one is the Finite Element Method (FEM), which is the basis of different commercial software, such as ADINA or ANSYS, among many others. The disadvantage of this method is the great amount of computational resources and iteration times required to obtain an accurate solution of the problem.

Given this disadvantage, Hughes developed the IsoGeometric Analysis (IGA). This method can integrate the CAD model with the Finite Element Analysis (FEA), thereby reduces the times and resources needed to obtain the precise solution. But in its turn, IGA lacks flexibility to obtain the solutions of certain problems because it uses the same basis functions to parameterize both, the geometry and the solution field.

Because of the latter, the Geometry Independent Field approximaTion (GIFT) was proposed as a generalization of IGA, which utilizes different basis functions to parameterize the geometry of the object and the solution field, allowing the selection of functions that adapt better to the problem studied. The previous work on GIFT was done for problems of Laplace's Equation and Linear Elasticity.

The main objective of this work is to further study the performance of GIFT for problems of bending and vibration of thin plates. The study consists in implementing GIFT for 3 different plates and comparing the numerical results with the analytical solutions of the Kirchhoff-Love Plate Theory (KLPT). A simple circular geometry plate, a circular two-patch geometry plate and a square plate with a cut-out of a complex shape, modeled by 8 patches, are considered. While all plates are parameterized by NURBS, the solutions are approximated by one patch NURBS or B-Splines. The results are demonstrated in terms of the convergence curves, vibrations modes and natural frequencies.

The numerical results are compared with the analytical solutions for problems with simple geometry and with the FEM solution for the problem of a plate of complex shape. The conducted analysis indicates that, *for the same (smooth) geometry parameterization*, (a) the solution can be approximated by one patch NURBS or B-Splines, while keeping the original geometry unaltered, (b) the results obtained with NURBS and B-Splines field approximations are quasi-identical, (c) the convergence rate depends on the degree of the solution approximation. For non-uniform geometry parameterizations, the method doesn't produce an optimal convergence rate or sufficiently accurate results, just like the traditional IGA.

To my family, my girlfriend and my friends,
"Learning never exhausts the mind."
Leonardo da Vinci

Agradecimientos

Agradezco a cada una de las personas que formaron parte de mi vida universitaria y parte de mi formación como ingeniero civil mecánico de esta universidad; especialmente a mis padres, Angélica y Eduardo, que han sido el soporte fundamental de mi vida, ya que siempre me han alentado y apoyado en todo para lograr cada una de mis metas. Los amo mucho y les estoy eternamente agradecido por todo lo que me han brindado, desde los valores que me inculcaron desde pequeño hasta los sacrificios que han hecho por mi para hacerme feliz y evitar que me faltase algo durante mi vida.

También a dos personas que han llegado a ser parte fundamental de mi vida: mi polola, Carolina Bernuy, y mi mejor amigo, Max Erazo. Carolina, durante esta última etapa, me ha apoyado incondicionalmente, me ha dado las fuerzas para seguir adelante y me ha apañado en todo, desde salidas hasta ayudarme con la memoria; además de llenarme de amor y felicidad. Mientras que Max, ha sido la persona con la cual he compartido más de 12 años de gran amistad y con la cual sé que puedo contar para cualquier cosa; juntos hemos vivido grandes y divertidos momentos, los que siempre recordaré y atesoraré.

Quiero agradecer a "Los Apuñalados", mis entrañables amigos del liceo, con los cuales he compartido y disfrutado de innumerables recuerdos. Sé que siempre podré contar con ellos y que nuestra amistad durará por siempre, los quiero mucho cabros.

Durante mi paso por la universidad conocí y compartí con varias personas, pero destaco a las amistades que formé en mecánica, especialmente a los Tropikalisimos. Dentro de este grupo, hago mención especial a Miguel Inostroza, Sebastián Goza y Maximiliano Pérez, quienes fueron los primeros a los que conocí y que siempre han sido buena onda conmigo. También quiero agradecer a Moisés Hueche, con quién compartí más tiempo a lo largo de la carrera y con el cual vivimos largas jornadas de estudio. Lo considero una gran persona y un gran amigo, agradezco toda la ayuda y buena onda que me brindó.

Hago un agradecimiento especial a la Profesora Elena, que sin ella no hubiese sido posible terminar la memoria, ya que siempre tuvo buena disposición para ayudarme con los problemas que surgían de ésta y que me apoyó para sacarla adelante. Vale mencionar nuevamente a Maximiliano Pérez, quién me ayudó bastante durante esta última etapa.

Finalmente, quiero hacer una mención a los miembros de la sala de memoristas del 5to, por hacer que cada día de trabajo en compañía de ustedes fuese más ameno y muchas gracias por toda la buena onda y ayuda brindada durante este último semestre.

Contents

List of Tables

List of Figures

Introduction and Motivation

There are different phenomena present in science and engineering, such as heat transfer, wave propagation or fluid movement, which are described by Partial Differential Equations (PDE), which, in many cases can not be solved by analytical methods. There are two alternatives to obtain such solutions: the first is to make a series of assumptions that allow to idealize and simplify the problem until it is possible to solve it analytically; while the other alternative is to use numerical methods that allow obtaining an approximate solution of the real problem.

The Finite Element Method (FEM) is one of the most popular methods of numerical analysis and used worldwide in the different areas of engineering, since it allows finding an approximate solution to various physical problems, such as: vibrations, kinematics and dynamics of fluid, heat transfer, wave propagation, deformations, among others. This method is the basis of a vast amount of programs available in the market, such as: ADINA, ANSYS, Comsol, etc. However, when the FEM analysis is performed on the CAD geometry model, the FEM software receives the geometry of a CAD model and converts it to the FEM model by means of discretization and re-parameterization of the boundaries.

FEM consists in dividing the geometry of an object into a finite number of elements, approximating the computational domain and the solution by polynomial shape functions within each element and reducing the problem to a set of local equations connected to each other. If the accuracy of the numerical solution is not satisfactory, the mesh of the model must be refined and in each refinement it is necessary to communicate with the CAD model to re-parameterize the geometry. This procedure increases the computational resources and the iteration time. Figure 1 shows a CAD model with its respective meshing and refinement of it.

To overcome these difficulty a new method of analysis emerged, the IsoGeometric Analysis (IGA), developed by Hughes et al. [1].

The IGA is a numerical method that allows to integrate the CAD models that use NURBS functions to represent the geometry with the Finite Element Analysis (FEA). Unlike the FEM, IGA avoids the approximation of the objects and works directly with its CAD geometry. The main idea of the method is to use the same basis functions to parameterize the geometry of the body and to approximate the unknown solution field. This allows to reduce computational and time resources; but it has certain disadvantages, such as: (a) lack of local refinement due to the tensor-product structure of NURBS and (b) the need to couple multi-patch geometries. In Figure 2 can be observed the main idea of the IGA schematically.

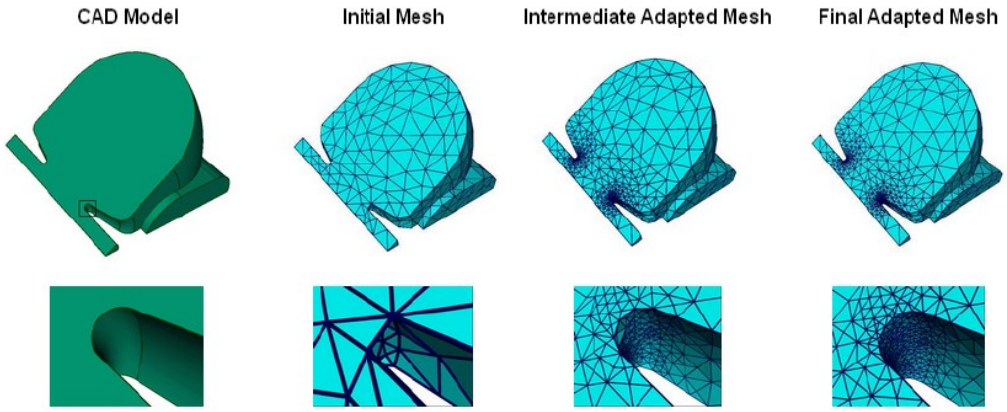

Figure 1: CAD model, meshing and refinement [1].

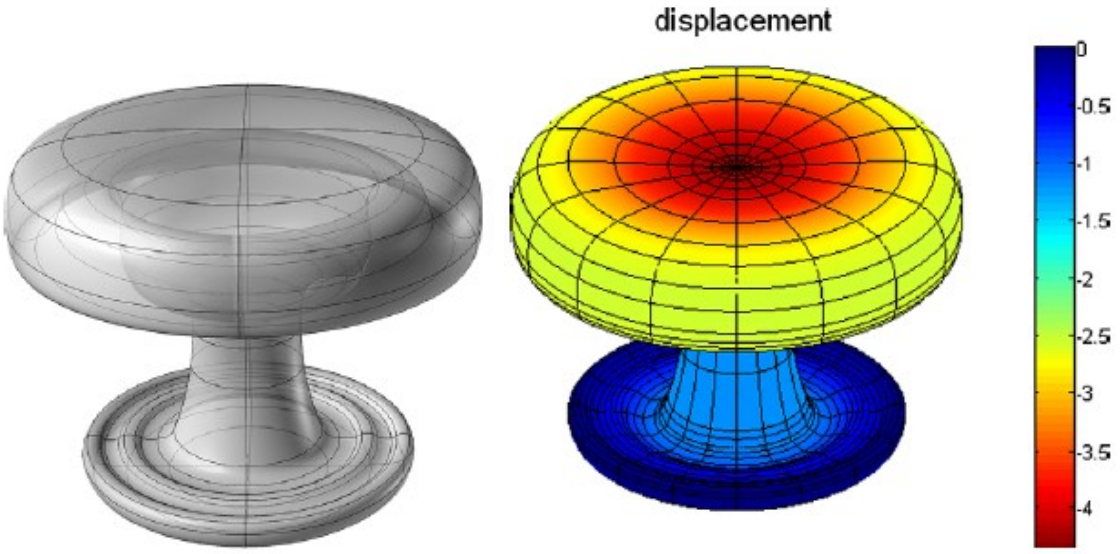

(a) Input IGA: CAD Model. (b) Output IGA: Displacement Distribution.

Figure 2: The main idea of the IsoGeoemtric Analysis (IGA) [2].

In order to overcome this lack of flexibility and adaptability, the Geometry Independent Field approximaTion (GIFT) was proposed in [3]. The GIFT is a generalization of the IGA and inherits the main advantage of it, which consists in preserving the original parametrization of the geometry of the CAD model; but allowing the use of other functions as the basis for the solution approximation. One can choose functions that are more convenient for the analysis, as, for example, B-Splines or PHT-Splines. It has been shown in [3] that the convergence rate of the method does not depend on the parameterization of the geometry and is fully defined by the polynomial order of the basis function of the solution approximation.

In [3] the performance of the method was demonstrated for Laplace's equation and linear elasticity, i.e. the PDEs of second order. The main idea of this work is to investigate the performance of GIFT when applied to problems of plate vibrations, based on Kirchhof-Love Plate Theory, described by the PDEs of 4-th order. The motivation of this thesis work is to show how the different options to parameterize the geometry and the solution field affect

the precision and the convergence rate of solution, both in terms of displacements as well as the natural frequencies for geometries composed of one or several patches and of various complexities.

For this, 3 plate problems are studied. The first one corresponds to a circular plate, with the analytical solution available to verify the implementation of the method. The second one is the same problem for a circular plate, but given by a two-patch NURBS parameterization. This problem serves to show how a simple but yet composite geometry can be analyzed using the GIFT method. The third problem is a realistic CAD geometry, i.e. a square plate with a cut-out of complex shape, parameterized by 8 NURBS patches. This problem demonstrates how this NURBS parameterization can be paired with a one-patch B-Splines solution field without any need for coupling the NURBS patches, like it is done in the standard IGA.

Chapter 1

Objectives and Scope

1.1 General Objective

The main objective of this work is to implement and validate the method of Geometry Independent Field approximaTion (GIFT) for the study of plate bending and vibrations, based on the Kirchhoff-Love Plate Theory (KLPT).

1.2 Specific Objectives

1. Modify and implement the GIFT algorithm for the study of thin plates.
2. Design three test cases based on three different NURBS geometry parameterizations.
3. Compare numerical data with analytical results, as well as the FEM solution for the plate of complex geometry, in terms of the convergence rate, vibration modes and natural frequencies.
4. Assess the performance of the method, based on the obtained results. Draw conclusions, analyze strengths and weaknesses of the GIFT method, formulate recommendations for potential users.

1.3 Scope

1. The work is restricted to applying the GIFT algorithm only to the study of KLPT plates. Other types of modifications to the existing code are not considered.
2. In this work, only 3 plates will be studied, which have 3 different geometries and characteristics between them.
3. Extension of the work to other plates theories, as well as other numerical methods, is not considered.

Chapter 2

Theoretical Background

In this section, the general and specific background information on which the thesis work is based will be presented and detailed.

2.1 Finite Element Method (FEM)

The Finite Element Method (FEM) is used to solve, numerically and roughly, physical problems necessary for engineering design and analysis. The FEM procedure is shown schematically in Figure 2.1 [4].

This method uses the following steps [5]:

1. **Domain Discretization:** it consists of dividing the object to study in a finite number of elements, where each element is formed by nodes that are in turn connected to the nodes of the nearby elements.
2. **Approximate Solution:** the variable under study is approximated by means of shape functions in each element.
3. **Finite Element Model:** it consists of transforming the problem to a set of local equations in each element that can be written in the following form:

$$[K_{\mathrm{e}}] \cdot \{u_{\mathrm{e}}\} = \{f_{\mathrm{e}}\} \tag{2.1}$$

   Where K_{e} represents the Elemental Stiffness Matrix, u_{e} is the vector of unknown nodal values in an element and f_{e} is the vector of Elemental Nodal Forces.
4. **Element Connectivity:** it consists in joining and assembling the equations of each of the elements, obtained in the previous stage; whereby the global equation of the problem is given by:

$$[K_g] \cdot \{u_g\} = \{f_g\} \tag{2.2}$$

   Where K_g represents the Global Stiffness Matrix, u_g is the global unknowns vector and f_g is the Global Nodal Forces Vector, the boundary conditions of the Neumann type are added to this last.

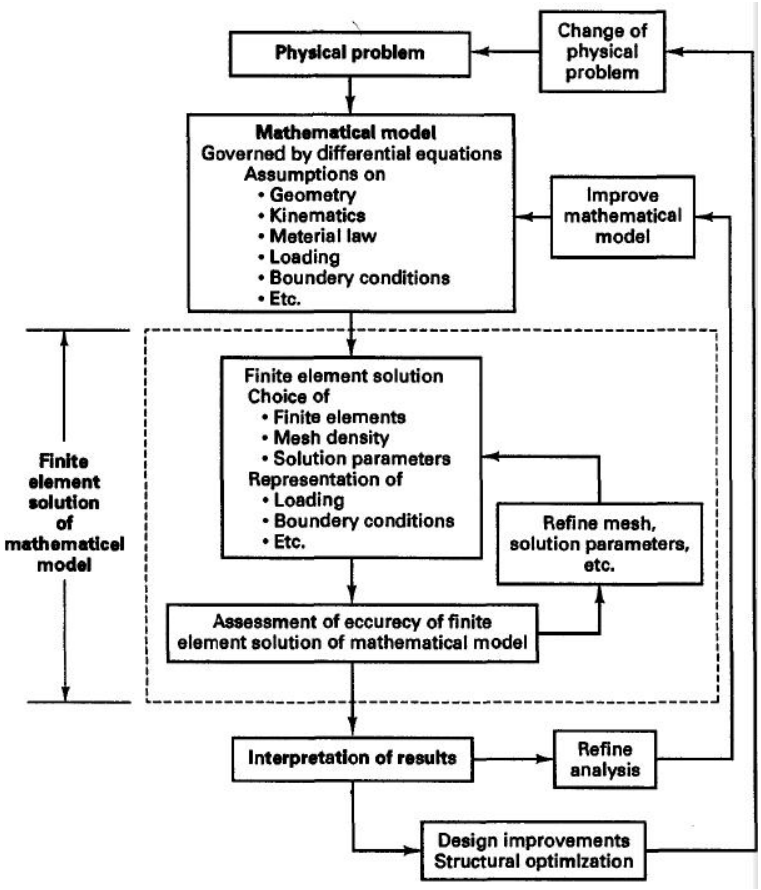

Figure 2.1: The process of Finite Element Method (FEM) [4].

5. **Imposition of Boundary Conditions:** the boundary conditions of the Dirichlet type are applied.
6. **Problem Resolution:** the global equation of the system is solved, the solution is given by:
$$\{u_g\} = [K_g]^{-1} \cdot \{f_g\} \tag{2.3}$$
7. **Post-Processing:** the results obtained are compared and analyzed in order to verify that the numerical solution is accurate enough (for example, by comparing it with the analytical solution). In the case if this precision is not achieved, the entire process must be repeated, but this time refining the mesh, that is, increasing the number of elements that discretize the domain of the problem, as can be seen in Figure 2.2.

2.2 IsoGeometric Analysis (IGA)

IsoGeometric Analysis (IGA) is a computational approach that allows the integration of Finite Element Analysis (FEA) with CAD design tools, based on NURBS (Non-Uniform Rational B-Splines). When using the FEA on CAD models, it is necessary to convert the CAD data to the FEA data, i.e. to re-parameterize the boundaries of CAD objects with the polynomials used in FEM. This procedure must be repeated during the solution refinement

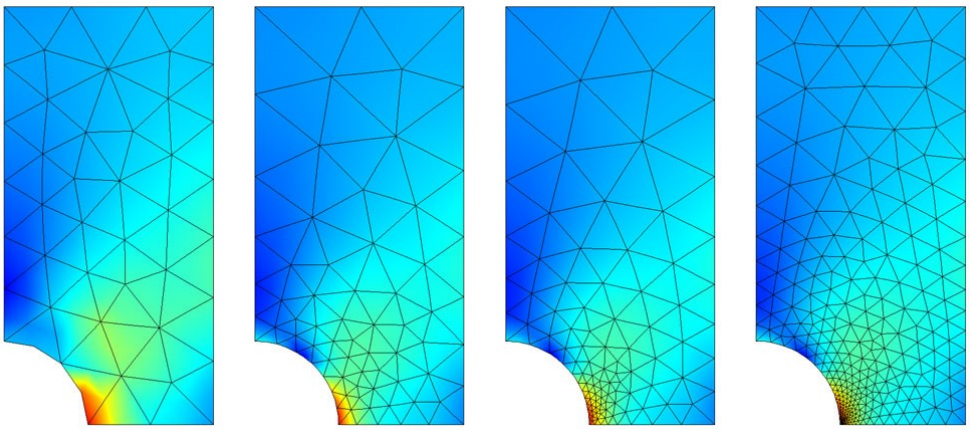

Figure 2.2: Refinement of the mesh when using FEM [4].

process. IGA allows to use CAD geometries directly for the finite element analysis. This allows the models to be designed, tested and adjusted at one time using a common data set [1]. This is achieved by utilizing the same shape functions, which are used in CAD to represent the geometries, to approximate the unknown fields.

The main idea of the IGA is shown schematically in Figure 2.3:

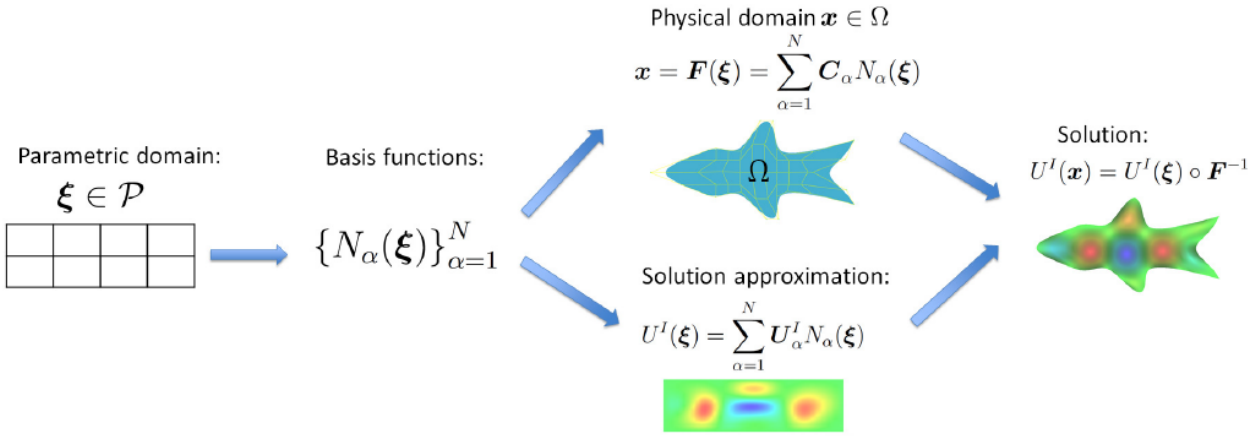

Figure 2.3: Main Idea of the IGA: the same shape functions are used both to parameterize the geometry of the object and to approximate the solution [3].

The bases of the IGA are detailed below:

2.2.1 B-Splines

Knot Vectors

A knot vector in one dimension is a set of coordinates in the parametric space, written $\Xi = \{\xi_1, \xi_2, ..., \xi_{n+p+1}\}$, where $\xi_\mathrm{i} \in \mathbb{R}$ is the i$-$th knot, i is the knot index, i $= 1, 2, ..., n+p+1$, p is the polynomial order, and n is the number of basis functions which comprise the B-Spline.

Basis Functions

B-Spline [6] basis functions are defined recursively starting with piecewise constants (p=0):

$$N_{\mathrm{i},0}(\xi) = \begin{cases} 1 & \text{if } \xi_{\mathrm{i}} \leq \xi \leq \xi_{\mathrm{i}+1} \\ 0 & \text{otherwise} \end{cases} \tag{2.4}$$

For p = 1, 2, 3, ..., are defined as follows:

$$N_{\mathrm{i},p}(\xi) = \frac{\xi - \xi_{\mathrm{i}}}{\xi_{\mathrm{i}+p} - \xi_{\mathrm{i}}} N_{\mathrm{i},p-1}(\xi) + \frac{\xi_{\mathrm{i}+p+1} - \xi}{\xi_{\mathrm{i}+p+1} - \xi_{\mathrm{i}-1}} N_{\mathrm{i}+1,p-1}(\xi) \tag{2.5}$$

The properties of the basis functions of the B-Splines are:

1. The basis functions constitute a partition of the unit, that is, $\forall \xi$:

$$\sum_{\mathrm{i}=1}^{n} N_{\mathrm{i},p}(\xi) = 1 \tag{2.6}$$

2. The support of each $N_{\mathrm{i},p}(\xi)$ is compact and contained in the interval $[\xi_{\mathrm{i}}, \xi_{\mathrm{i}+p+1}]$.
3. Each basis function is non-negative, that is, $N_{\mathrm{i},p}(\xi) \geq 0, \forall \xi$. Consequently, all of the coefficients of a mass matrix computed from a B-spline basis are greater than, or equal to, zero.

B-Spline Curves

B-Spline curves in $\mathbb{R}^{\mathrm{d}}$, $\mathrm{d} = 2, 3$, are constructed by taking a linear combination of B-Spline basis functions. The coefficients of the basis functions are referred to as control points. These are somewhat analogous to nodal coordinates in finite element analysis. Piecewise linear interpolation of the control points gives the so-called control polygon. In general, control points are not interpolated by B-spline curves. Given n basis functions, $N_{\mathrm{i},p}$, i = 1, 2,..., n, and corresponding control points $\mathbf{B_i} \in \mathbb{R}^{\mathrm{d}}$, i = 1, 2,..., n; a piecewise-polynomial B-Spline curve is given by:

$$\mathbf{C}(\xi) = \sum_{\mathrm{i}=1}^{n} N_{\mathrm{i},p}(\xi) \mathbf{B_i} \tag{2.7}$$

An example of a B-Splines curve is shown in Figure 2.4 for the quadratic basis functions shown in the same figure.

The properties of the B-Splines curves are:

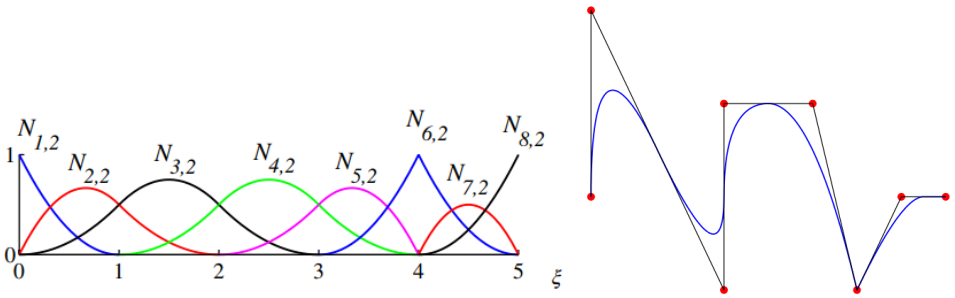

(a) Quadratic basis function for the knot vector $\Xi = \{0, 0, 0, 1, 2, 3, 4, 4, 5, 5, 5\}$.

(b) B-Spline piecewise quadratic curve in $\mathbb{R}^2$.

Figure 2.4: Example for a B-Spline curve [6].

1. They have continuous derivatives of order $p - 1$ in the absence of repeated knots or control points.
2. Repeating a knot or control point k times decreases the continuity of the derivatives to $p - k$.
3. An affine transformation of a B-spline curve is obtained by applying the transformation to the control points, this property is called as affine covariance.

B-Splines Surfaces

Given a control net $\{\mathbf{B_{i,j}}\}$, i = 1, 2,. . . , n, j = 1, 2,. . . , m, and knot vectors Ξ=$\{\xi_1, \xi_2, ..., \xi_{n+p+1}\}$, and H=$\{\eta_1, \eta_2, ..., \eta_{m+q+1}\}$, a tensor product B-Spline surface is defined by:

$$\mathbf{S}(\xi, \eta) = \sum_{\mathrm{i}=1}^{n} \sum_{j=1}^{m} N_{\mathrm{i},p}(\xi) M_{j,q}(\eta) \mathbf{B_{i,j}} \tag{2.8}$$

Where $N_{\mathrm{i},p}$ and $M_{j,q}$ are basis functions of B-Spline curves. For purposes of numerically integrating arrays constructed from B-Splines, elements are taken to be knot spans, namely, $[\xi_{\mathrm{i}}, \xi_{\mathrm{i}+1}] \times [\eta_{\mathrm{i}}, \eta_{\mathrm{i}+1}]$.

B-Splines Solids

Tensor product B-Spline solids are defined in analogous fashion to B-spline surfaces. Given a control net $\{\mathbf{B_{i,j,k}}\}$, i = 1, 2,. . . , n, j = 1, 2,. . . , m, k = 1, 2,. . . , l, and knot vectors Ξ=$\{\xi_1, \xi_2, ..., \xi_{n+p+1}\}$, H=$\{\eta_1, \eta_2, ..., \eta_{m+q+1}\}$ and $\mathfrak{L}$=$\{\zeta_1, \zeta_2, ..., \zeta_{l+r+1}\}$; a B-Spline solid is defined by:

$$\mathbf{V}(\xi, \eta, \zeta) = \sum_{\mathrm{i}=1}^{n} \sum_{j=1}^{m} \sum_{k=1}^{l} N_{\mathrm{i},p}(\xi) M_{j,q}(\eta) L_{k,r}(\zeta) \mathbf{B_{i,j,k}} \tag{2.9}$$

2.2.2 NURBS (Non-Uniform Rational B-Splines)

The rational basis functions and NURBS [1] curve are given, respectively, by:

$$R_{\mathrm{i}}^{p}(\xi) = \frac{N_{\mathrm{i},p}(\xi) w_{\mathrm{i}}}{\sum_{\mathrm{i}=1}^{n} N_{\mathrm{i},p}(\xi) w_{\mathrm{i}}} \tag{2.10}$$

$$\mathbf{C}(\xi) = \sum_{\mathrm{i}=1}^{n} R_{\mathrm{i}}^{p}(\xi) \mathbf{B_i} \tag{2.11}$$

Rational surfaces and solids are defined analogously in terms of the rational basis functions:

$$R_{\mathrm{i},j}^{p,q}(\xi,\eta) = \frac{N_{\mathrm{i},p}(\xi) M_{j,q}(\eta) w_{\mathrm{i},j}}{\sum_{\mathrm{i}=1}^{n} \sum_{j=1}^{m} N_{\mathrm{i},p}(\xi) M_{j,q}(\eta) w_{\mathrm{i},j}} \tag{2.12}$$

$$R_{\mathrm{i},j,k}^{p,q,r}(\xi,\eta,\zeta) = \frac{N_{\mathrm{i},p}(\xi) M_{j,q}(\eta) L_{k,r}(\zeta) w_{\mathrm{i},j,k}}{\sum_{\mathrm{i}=1}^{n} \sum_{j=1}^{m} \sum_{k=1}^{l} N_{\mathrm{i},p}(\xi) M_{j,q}(\eta) L_{k,r}(\zeta) w_{\mathrm{i},j,k}} \tag{2.13}$$

Surfaces and solids NURBS are given, respectively, by:

$$\mathbf{S}(\xi,\eta) = \sum_{\mathrm{i}=1}^{n} \sum_{j=1}^{m} R_{\mathrm{i},j}^{p,q}(\xi,\eta) \mathbf{B_{i,j}} \tag{2.14}$$

$$\mathbf{V}(\xi,\eta,\zeta) = \sum_{\mathrm{i}=1}^{n} \sum_{j=1}^{m} \sum_{k=1}^{l} R_{\mathrm{i},j,k}^{p,q,r}(\xi,\eta,\zeta) \mathbf{B_{i,j,k}} \tag{2.15}$$

Figure 2.5 shows a control net and the corresponding NURBS surface description of a torus.

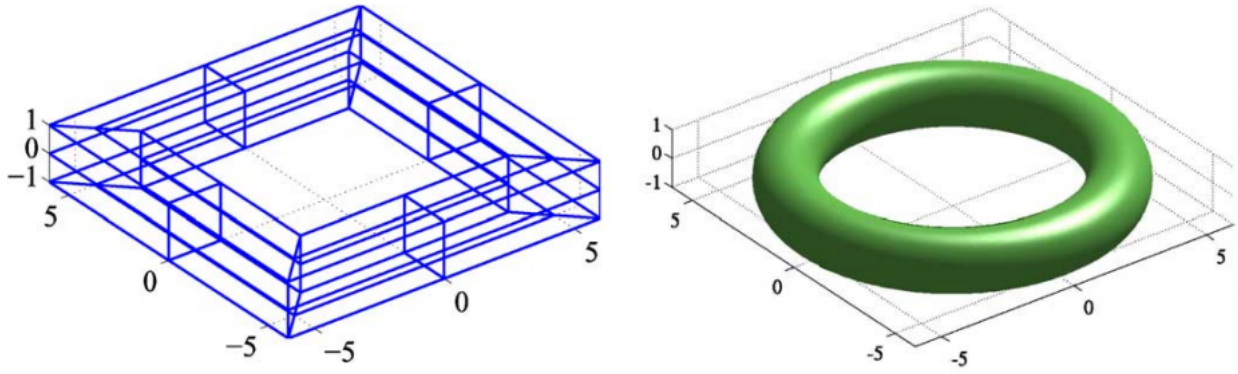

Figure 2.5: Control net for a toroidal surface and the toroidal surfaces generated [1].

The properties of the NURBS are:

1. NURBS basis functions form a partition of unity.
2. The continuity and support of NURBS basis functions are the same as for B-Splines.
3. Affine transformations in physical space are obtained by applying the transformation to the control points, that is, NURBS possess the property of affine covariance.
4. If weights are equal, NURBS become B-Splines (i.e., piecewise polynomials)
5. NURBS surfaces and solids are the projective transformations of tensor product, piecewise polynomial entities.
6. NURBS can accurately represent conical surfaces, such as: circles, parabolas, ellipses, among others.

A summary of similar and dissimilar Finite Element Analysis and IsoGeometric Analysis concepts is presented in Table 2.1 [1].

Table 2.1: Comparison of Finite Element Analysis and IsoGeometric Analysis based on NURBS [1].

Differences	
Finite Element Analysis (FEA)	IsoGeometric Analysis (IGA)
Nodal points	Control points
Nodal variables	Control variables
Mesh	Knots
Basis interpolates nodal points and variables	Basis does not interpolate control points and variables
Approximate geometry	Exact geometry
Polynomial basis	NURBS basis
Gibbs phenomena	Variation diminishing
Subdomains	Patches
Similarities	
Compact support	
Partition of unity	
Isoparametric concept	
Affine covariance	
Patch tests satisfied	

2.2.3 Refinement

An interesting feature of NURBS or B-Splines, among others, is that the shape functions space can be enhanced without modifying the geometry description and its parametrization. Three types of refinement exist, and for all of them, the space is enriched by adding control points to the geometry.

$h-$Refinement: Knot Insertion

The first refinement method presented here is knot insertion [7]. This is the IGA counterpart of the classical $h-$refinement strategy in standard FEM. Given a knot vector $\Xi = \{\xi_1, \xi_2, \cdots, \xi_{n+p+1}\}$, let us define an enriched knot vector:

$$\widetilde{\Xi} = \left\{\widetilde{\xi}_1 = \xi_1, \widetilde{\xi}_2, \cdots \widetilde{\xi}_{n+m+p+1} = \xi_{n+p+1}\right\} \tag{2.16}$$

Such that $\Xi \subset \widetilde{\Xi}$. Subsequently, the new $n+m$ basis are defined recursively as previous introduced, but this time they associated to the new knot vector $\widetilde{\Xi}$, see Figure 2.6. The new $m+n$ control points are computed as a linear combination of the original control points. The method is applicable directly to B-Splines, whereas for NURBS the same approach can be used but it has to be applied on the projective $\mathbb{R}^{n+1}$-dimensional B-Spline entity, from which the NURBS is derived.

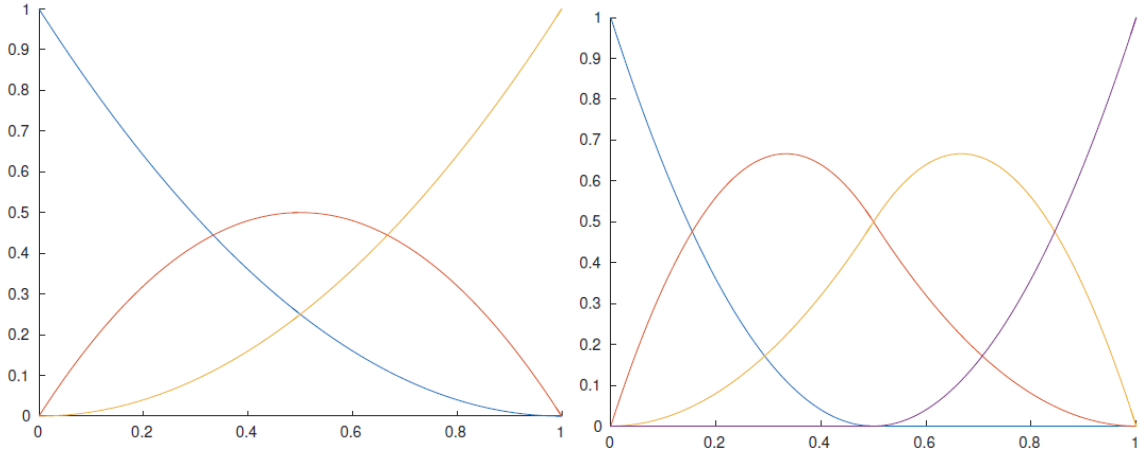

(a) $\Xi = \{0,0,0,1,1,1\}$ (b) $\widetilde{\Xi} = \{0,0,0,\frac{1}{2},1,1,1\}$

(c) $\overline{\Xi} = \{0,0,0,\frac{1}{2},\frac{1}{2},1,1,1\}$ (d) $\widehat{\Xi} = \{0,0,0,\frac{1}{2},\frac{1}{2},\frac{3}{4},1,1,1\}$

Figure 2.6: Basis functions before and after knot insertion, order $p = 2$. Note the changes in continuity at the knots, given as C^{p-k} [7].

p-Refinement: Order Elevation

The second refinement method is order elevation [7], which has similarities with the classical $p-$refinement strategy in standard FEM. This method involves increasing the polynomial order of the shape functions used to represent the geometry. In this approach, the continuity at every knot is preserved and therefore, during order elevation, existing knots multiplicity is increased by one, without adding any new knot. Analogously to knot insertion, neither the geometry nor the parametrization are changed after performing order elevation. In Figure 2.7, an example of shape functions after order elevation is depicted.

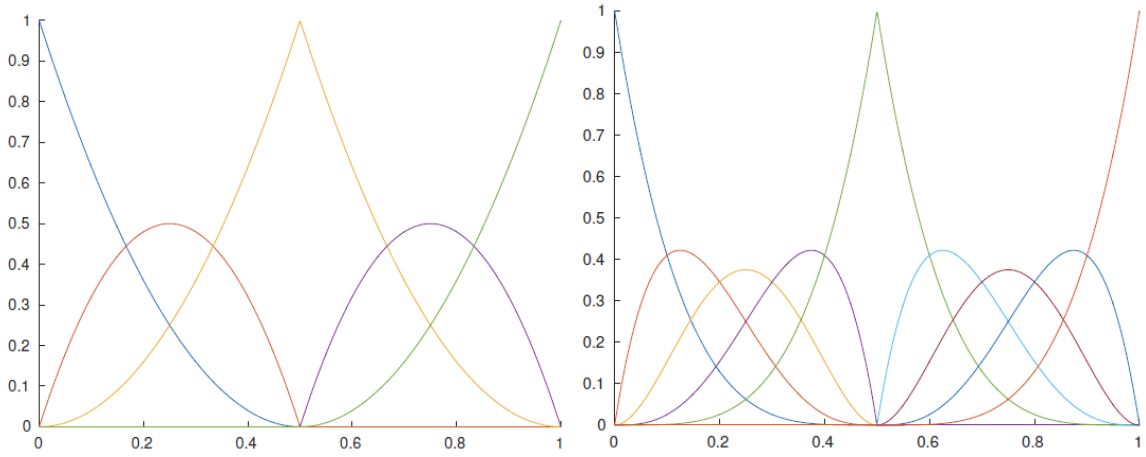

(a) $\Xi = \{0, 0, 0, \frac{1}{2}, \frac{1}{2}, 1, 1, 1\}$ (b) $\widetilde{\Xi} = \{0, 0, 0, 0, 0, \frac{1}{2}, \frac{1}{2}, \frac{1}{2}, \frac{1}{2}, 1, 1, 1, 1, 1\}$

Figure 2.7: Basis functions before and after order elevation, from $p = 2$ to $p = 4$. Note that the continuity at the knots is preserved as well as the number of distinct knot intervals [7].

$hp-$Refinement

The third method is the $hp-$ or $k-$refinement and it consists of a combined process of degree elevation and knot insertion. These processes are not commutative and therefore the order in which these refinements are applied will change the final basis. $hp-$refinement first applies degree elevation proceeded by knot insertion, offering a reduction in degrees of freedom over its counterpart [8].

2.3 Geometry Independent Field approximaTion (GIFT)

The Geometry Independent Field approximaTion (GIFT) [3] is a generalization of the concept of IsoGeometric Analysis (IGA), since it allows the coexistence of different spaces for the parametrization of the computational domain and for the approximation of the field of the solution. This means that this method allows to preserve the exact geometry of the CAD that uses for example, NURBS functions; but, in the approximation space of the solution, it

allows the use of more flexible and/or suitable functions for the analysis, such as: T-Splines, LR-Splines, Hierarchical B-Splines and PHT-Splines.

This generalization of the IGA allows a local refinement adapted without the need to re-parameterize the geometry of the domain given by the CAD model, as can be seen in Figure 2.8. This method was so far applied to problems of heat transfer (Poisson's equation) and linear elasticity.

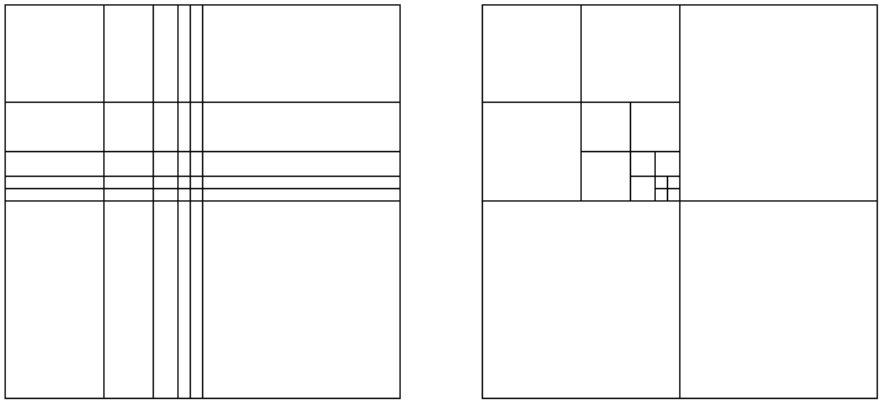

(a) Tensor-product mesh in the parametric space (global refinement).

(b) T-mesh in the parametric space (local refinement).

Figure 2.8: Refinements in the parametric space [3].

The main idea of GIFT is to preserve the original geometry of the CAD while adapting the base of the solution with flexibility and thus improving the approximation of the solution field. The main features of GIFT are:

1. Preserve exact CAD geometry provided in any form, including B-splines or NURBS, at any stage of the solution process.
2. Allow local refinement of the solution by choosing appropriate field approximations, as independently as possible of the geometrical parameterization of the domain.
3. Allow computational savings by not refining the geometry during the process of refining the solution and by choosing simpler approaches for the solution, that is, using polynomial functions instead of rational functions.

In Figure 2.9 one can see the main idea of the GIFT.

2.3.1 Formulation of GIFT

It is considered an open domain $\Omega \subset \mathbb{R}^{\mathrm{d}}$, $\mathrm{d} \geq 2$, with boundary Γ consisting of two parts (Γ_D and Γ_N), such that: $\Gamma{=}(\overline{\Gamma_D \cup \Gamma_N})$, $\Gamma_D \cap \Gamma_N = \emptyset$. The domain Ω is parameterized on a parametric domain P by mapping F:

$$F : P \rightarrow \Omega \qquad \boldsymbol{x} = F(\boldsymbol{\xi}) \qquad \boldsymbol{x} \in \Omega, \boldsymbol{\xi} \in P \tag{2.17}$$

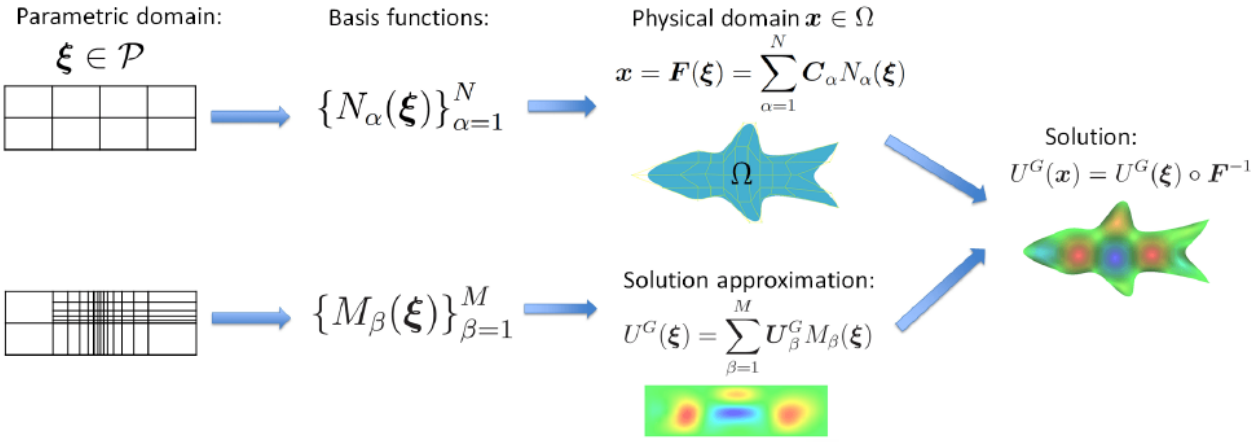

Figure 2.9: Main Idea of the GIFT: different basis functions are used to parameterize the geometry of the object and the approximation of the solution [3].

To be consistent with the previous notations, $\boldsymbol{\xi} = (\xi, \eta)$ in the two-dimensional case and $\boldsymbol{\xi} = (\xi, \eta, \zeta)$ in the three-dimensional case. Note, that the present work is limited to 2D plate problems. In what follows we also use collapsed indexes, for example $N_k(\boldsymbol{\xi})$, where $k = (\mathrm{i}, j)$. The NURBS basis functions are denoted as $N_k(\boldsymbol{\xi})$, while the B-Splines basis functions as $B_k(\boldsymbol{\xi})$.

The geometrical map F is given by a set of basis functions $N_{\mathrm{i}}(\boldsymbol{\xi})$ and a set of control points $\boldsymbol{C}_{\mathrm{i}}$, such that:

$$\mathbf{x}(\boldsymbol{\xi}) = F(\boldsymbol{\xi}) = \sum_{k \in I} \boldsymbol{C}_k N_k(\boldsymbol{\xi}) \tag{2.18}$$

In the framework of GIFT, one can choose different basis functions, $\{M_k(\boldsymbol{\xi})\}_{k \in J}$, to seek the solution in the form:

$$u(\boldsymbol{\xi}) = \sum_{k \in J} u_k M_k(\boldsymbol{\xi}) \tag{2.19}$$

Where u_k are the unknown control variables. If the weak form of the boundary value problem is given by:

$$a(u, v) = l(v), \tag{2.20}$$

using the representation (2.19) together with $v = M_j(\boldsymbol{\xi})$, the weak form (2.20) can be transformed to a linear system of equations:

$$\mathbf{Ku} = \mathbf{f} \tag{2.21}$$

where $\mathbf{K}$ correspond to the Global Stiffness Matrix, $\mathbf{u}$ is the vector of all unknown control variables u_k and $\mathbf{f}$ is the vector of Global Nodal Forces; which are given by:

$$K_{\mathrm{i},j} = a(M_{\mathrm{i}}(\boldsymbol{x}), M_j(\boldsymbol{x})) \qquad f_{\mathrm{i}} = l(M_{\mathrm{i}}(\boldsymbol{x})) \tag{2.22}$$

2.4 Kirchhoff-Love Plate Theory (KLPT)

The plates are defined as structures that have one dimension much smaller than the other two. Plate theory reduces the analysis of a 3-dimensional structure to a 2-dimensional problem. The equations that govern the plate theory are Partial Differential Equations (PDE) in two dimensions defined in the mid-plane of the plate.

The Kirchhoff-Love Plate Theory (KLPT) [9] is used for the analysis of thin plates, and which is based on assumptions that are closely related to the Euler-Bernoulli Beam Theory. The assumptions of the TPKL deal with the kinematics of a line of normal material, that is, a set of particles of material initially aligned in a direction normal to the mid-plane of the plate.

The fundamental assumption of the KLPT is that the line of normal material is infinitely rigid along its length, that is, no deformations occur in the direction normal to the middle plane of the plate. During deformation, it is assumed that the line of normal material remains straight and normal to the deformed mid-plane of the plate. The assumptions of the KLPT can be summarized in the following 3:

1. The normal material line is infinitely rigid along its own length.
2. The normal material line of the plate remains a straight line after deformation.
3. The straight normal material line remains normal to the deformed mid-plane of the plate.

Experimental measurements show that these assumptions are valid for thin plates made of homogeneous, isotropic materials. When one or more of theses conditions are not met, the predictions of Kirchhoff-Love Plate Theory might become inaccurate.

The KLPT is characterized by the following set of equations:

1. **Six Strain-Displacement Equations:** three equations define the mid-plane strains in terms of the plate in-plane displacements, see Equation (2.23), and three equations define the plate curvatures in terms of the transverse displacement, see Equation (2.24).

$$\underline{\varepsilon_o} = \left\{ \frac{\partial \overline{u}_1}{\partial x_1}, \frac{\partial \overline{u}_2}{\partial x_2}, \frac{\partial \overline{u}_1}{\partial x_2} + \frac{\partial \overline{u}_2}{\partial x_1} \right\}^T = \left\{ \varepsilon_1^0, \varepsilon_2^0, \varepsilon_{12}^0 \right\}^T \tag{2.23}$$

$$\underline{\kappa} = \left\{ \frac{\partial^2 \overline{u}_3}{\partial x_2^2}, -\frac{\partial^2 \overline{u}_3}{\partial x_1^2}, 2\frac{\partial^2 \overline{u}_3}{\partial x_1 \partial x_2} \right\}^T = \left\{ \kappa_1, \kappa_2, \kappa_{12} \right\}^T \tag{2.24}$$

Where, x_{i} denotes the i−th direction, $\overline{u}_{\mathrm{i}}$ is one of the displacement of the normal material line, $\underline{\varepsilon_o}$ and $\underline{\kappa}$ are the array of mid-plane strain and curvatures of the plates, respectively.

2. **Five Equilibrium Equations:** : two equations express the equilibrium conditions for the in-plane forces, see Equation (2.25), one equation expresses the vertical force equilibrium condition, see Equation (2.26); and two equations express the moment equilibrium conditions, see Equation (2.27).

$$\frac{\partial N_1}{\partial x_1} + \frac{\partial N_{12}}{\partial x_2} = -p_1 \qquad \frac{\partial N_{12}}{\partial x_1} + \frac{\partial N_2}{\partial x_2} = -p_2 \tag{2.25}$$

$$\frac{\partial Q_1}{\partial x_1} + \frac{\partial Q_2}{\partial x_2} = -p_3 \tag{2.26}$$

$$\frac{\partial M_2}{\partial x_1} - \frac{\partial M_{12}}{\partial x_2} - Q_1 = 0 \qquad \frac{\partial M_{12}}{\partial x_1} + \frac{\partial M_1}{\partial x_2} + Q_2 = 0 \tag{2.27}$$

Where, N denotes to the in-plane forces, p_{i} is an in-plane pressure acting along the i−th direction, Q denotes to the transverse shear forces and M corresponding to the bending moments

3. **Six Constitutive Laws:** three equations state the relationship between the in-plane forces and mid-plane strains, see Equation (2.28), and three equations state the relationship between the bending moments and plate curvatures, see Equation (2.29).

$$\underline{N} = \{N_1, N_2, N_{12}\}^T = h\underline{\underline{C}}\underline{\varepsilon_o} = \frac{hE}{(1+\nu)(1-2\nu)} \begin{bmatrix} 1-\nu & \nu & 0 \\ \nu & 1-\nu & 0 \\ 0 & 0 & \dfrac{1-\nu}{2} \end{bmatrix} \underline{\varepsilon_o} \tag{2.28}$$

$$\underline{M} = \{M_1, M_2, M_{12}\}^T = \underline{\underline{\widetilde{D}}}\underline{\kappa} = \frac{Eh^3}{12(1-\nu^2)} \begin{bmatrix} 1 & -\nu & 0 \\ -\nu & 1 & 0 \\ 0 & 0 & \dfrac{1-\nu}{2} \end{bmatrix} \underline{\kappa} \tag{2.29}$$

Where, $\underline{N}$ and $\underline{M}$ are the array of in-plane forces and bending moments, respectively.

Figures 2.10, 2.11 and 2.12 respectively show the acting forces and free-body diagrams with the balances of external forces, shear stresses and moments of deflection on a differential element of a plate.

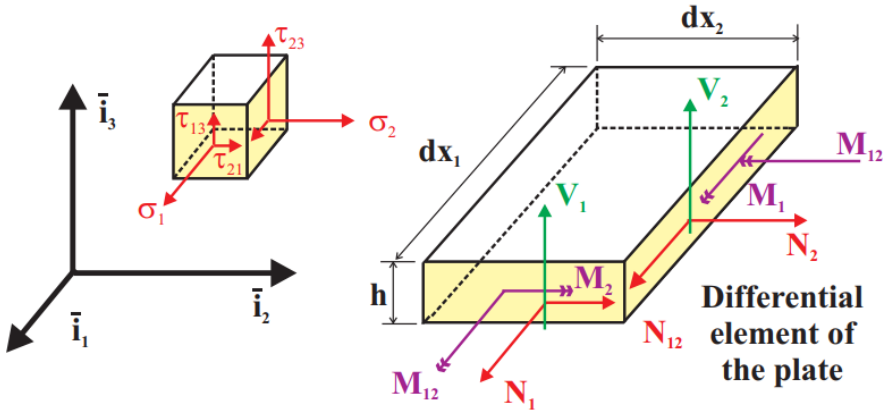

Figure 2.10: Stress resultants acting on a differential element of the plate [9].

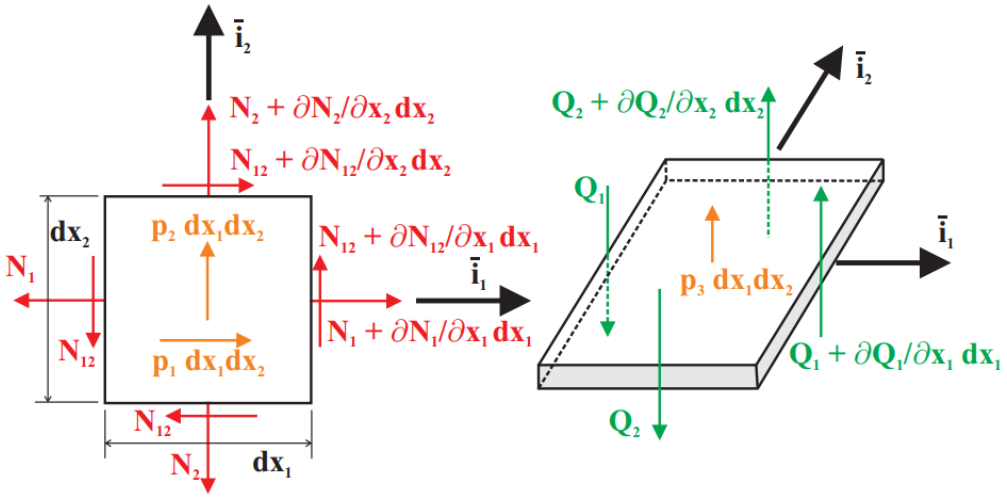

Figure 2.11: (Left) Free body diagram for the equilibrium of in-plane forces. (Right) Free body diagram for the equilibrium of transverse shear forces.[9].

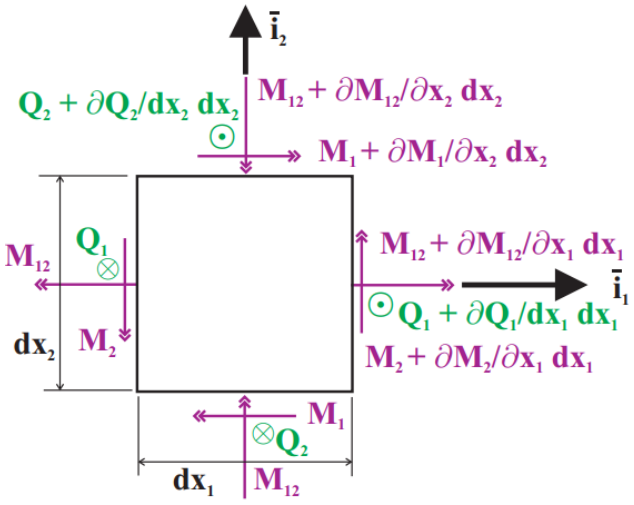

Figure 2.12: Free body diagram for the equilibrium of bending moment and shear forces [9].

2.4.1 The Bending Problem of the KLPT

This set of seventeen equations allow to reduce the bending problem to a single partial differential equation for the plate transverse displacement, $\overline{u}_3$.

This problem involves nine unknowns: the three bending moments, the two transverse shear forces, the three curvatures, and the transverse displacement; using the equations of the KLPT, the problem is reduced to an equation of the following type:

$$\frac{\partial^4 \overline{u}_3}{\partial x_1^4} + 2\frac{\partial^4 \overline{u}_3}{\partial x_1^2 \partial x_2^2} + \frac{\partial^4 \overline{u}_3}{\partial x_2^4} = \frac{p_3}{D} \tag{2.30}$$

$$D = \frac{Eh^3}{12(1-\nu^2)} \tag{2.31}$$

Where $\overline{u}_3 = w$ is the plate transverse displacement, D is the Plate Bending Stiffness, E and ν correspond to the Young's Modulus and the Poisson's Ratio of the material, h is the thickness of the plate and $p_3 = q$ is an external force per unit area.

The basic equation of Kirchhoff-Love Plate Bending Theory, Eq. (2.30), is the biharmonic partial differential equation for the transverse displacement, which can be written in a more compact manner with the help of the Laplacian operator $\nabla^4 = \nabla^2\nabla^2$ in two dimensions:

$$\nabla^4 w = \frac{q}{D} \tag{2.32}$$

2.4.2 The Vibration Problem of the KLPT

The Partial Differential Equation that describes the free vibrations of a plate subjected to external load is the following [10]:

$$D\nabla^2\nabla^2 w + \rho h\frac{\partial^2 w}{\partial t^2} = q \tag{2.33}$$

The additional parameters are: ρ - the density of the material, q - the external force applied to the mean surface, distributed transversally per unit area.

The Laplacian operator ∇^2 in Cartesian coordinates (x, y) and in cylindrical coordinates (r, θ) for two dimensions is defined, respectively, as [11]:

$$\nabla^2 w(x, y) \equiv \frac{\partial^2 w}{\partial x^2} + \frac{\partial^2 w}{\partial y^2} \tag{2.34}$$

$$\nabla^2 w(r,\theta) \equiv \frac{1}{r}\frac{\partial}{\partial r}\left(r\frac{\partial w}{\partial r}\right) + \frac{1}{r^2}\frac{\partial^2 w}{\partial \theta^2} \tag{2.35}$$

2.4.3 Weak Form of the Kirchhoff-Love Plate Theory

The weak form of the Kirchhoff-Love Plate Theory [12] is:

$$\begin{aligned} &D\int_\Omega \left[\frac{\partial^2 w}{\partial x^2}\frac{\partial^2 v}{\partial x^2} + \nu\left(\frac{\partial^2 w}{\partial x^2}\frac{\partial^2 v}{\partial y^2} + \frac{\partial^2 w}{\partial y^2}\frac{\partial^2 v}{\partial x^2}\right) + \frac{\partial^2 w}{\partial y^2}\frac{\partial^2 v}{\partial y^2} + 2\left(1-\nu\right)\frac{\partial^2 w}{\partial x \partial y}\frac{\partial^2 v}{\partial x \partial y}\right] d\Omega \\ &= \int_\Omega q v \, d\Omega + \int_{\partial\Omega} \overline{q} v \, d\partial\Omega - \int_{\partial\Omega} \overline{m}_{nm}\frac{\partial v}{\partial n} d\partial\Omega - \sum_{\mathrm{i}=1}^{N} \left[R_{P_\mathrm{i}} v\right]_{P_\mathrm{i}} \end{aligned} \tag{2.36}$$

Where:

- v: is the test function.
- q: transversal distributed load to the domain Ω.
- $\overline{q}$: transversal distributed load to the mean surface on the boundary $\partial\Omega$ of domain Ω.
- $\overline{m}_{nm}$: distributed moment in the tangent direction t of boundary $\partial\Omega$.
- R_{P_i}: concentrated forces in the transversal direction of the plate on points P_i of the boundary with geometrical discontinuities
- n: normal direction to the boundary $\partial\Omega$.

While the strong form of KLPT, see Eq. (2.32) or (2.33), has derivatives up to the fourth order, the weak form only has second-order derivatives. Therefore, functions w and v have to belong to the set $C^1(x,y)$ (continuous functions with continuous first-order partial derivatives) or $C^1_{cp}(x,y)$ (piecewise continuous first-order derivatives). In the strong form, these functions must be continuous in $C^4(x,y)$ or piecewise continuous in $C^4_{cp}(x,y)$.

If the approximate solution $w(x,y)$ for the transverse displacement of the Kirchhoff plate is given by the following linear combination of N global basis functions $\{N_\mathrm{i}\}_{\mathrm{i}=1}^{N}$, like the Eq. (2.19):

$$w(x,y) = \sum_{\mathrm{i}=1}^{N} u_\mathrm{i} N_\mathrm{i}(x,y) \tag{2.37}$$

While for $v(x,y)$:

$$v(x,y) = \sum_{j=1}^{n} b_\mathrm{i} N_j(x,y) \tag{2.38}$$

The approximation of the weak form of the Kirchhoff-Love Plate Theory is the following:

$$\sum_{\mathrm{i},j=1}^{N}\left\{D\int_{\Omega}\left[\frac{\partial^2 N_{\mathrm{i}}}{\partial x^2}\frac{\partial^2 N_j}{\partial x^2}+\nu\left(\frac{\partial^2 N_{\mathrm{i}}}{\partial x^2}\frac{\partial^2 N_j}{\partial y^2}+\frac{\partial^2 N_{\mathrm{i}}}{\partial y^2}\frac{\partial^2 N_j}{\partial x^2}\right)+\frac{\partial^2 N_{\mathrm{i}}}{\partial y^2}\frac{\partial^2 N_j}{\partial y^2}+2\left(1-\nu\right)\frac{\partial^2 N_{\mathrm{i}}}{\partial x\partial y}\frac{\partial^2 N_j}{\partial x\partial y}\right]d\Omega\right\}u_{\mathrm{i}}$$
$$=\int_{\Omega}qN_j\,d\Omega+\int_{\partial\Omega}\overline{q}N_j\,d\partial\Omega-\int_{\partial\Omega}\overline{m}_{nm}\frac{\partial N_j}{\partial n}\,d\partial\Omega-\sum_{\mathrm{i}=1}^{N}\left[R_{P_{\mathrm{i}}}N_j\right]_{P_{\mathrm{i}}} \tag{2.39}$$

This equation represents the system of linear equations of the form:

$$\mathbf{Ku}=\mathbf{f} \tag{2.40}$$

Where, the coefficients of the Global Stiffness Matrix $\mathbf{K}$ and the Force Vector $\mathbf{f}$ are given, respectively, by :

$$K_{\mathrm{i}j}=D\int_{\Omega}\left[\frac{\partial^2 N_{\mathrm{i}}}{\partial x^2}\frac{\partial^2 N_j}{\partial x^2}+\nu\left(\frac{\partial^2 N_{\mathrm{i}}}{\partial x^2}\frac{\partial^2 N_j}{\partial y^2}+\frac{\partial^2 N_{\mathrm{i}}}{\partial y^2}\frac{\partial^2 N_j}{\partial x^2}\right)+\frac{\partial^2 N_{\mathrm{i}}}{\partial y^2}\frac{\partial^2 N_j}{\partial y^2}+2\left(1-\nu\right)\frac{\partial^2 N_{\mathrm{i}}}{\partial x\partial y}\frac{\partial^2 N_j}{\partial x\partial y}\right]d\Omega \tag{2.41}$$

$$f_j=\int_{\Omega}qN_j\,d\Omega+\int_{\partial\Omega}\overline{q}N_j\,d\partial\Omega-\int_{\partial\Omega}\overline{m}_{nm}\frac{\partial N_j}{\partial n}\,d\partial\Omega-\sum_{\mathrm{i}=1}^{N}\left[R_{P_{\mathrm{i}}}N_j\right]_{P_{\mathrm{i}}} \tag{2.42}$$

The coefficients of the global stiffness matrix can also be denoted by the following matrix product [13]:

$$K_{\mathrm{i}j}=\int_{\Omega}\mathbf{B}_{\mathrm{i}}^{T}\mathbf{D}\mathbf{B}_j\,d\Omega \tag{2.43}$$

The stress-displacement vector is given by:

$$\mathbf{B}_{\mathrm{i}}^{T}=\begin{Bmatrix}-\dfrac{\partial^2 N_{\mathrm{i}}}{\partial x^2} & -\dfrac{\partial^2 N_{\mathrm{i}}}{\partial y^2} & -\dfrac{\partial^2 N_{\mathrm{i}}}{\partial x\partial y}\end{Bmatrix}^{T} \tag{2.44}$$

The elasticity matrix $\mathbf{D}$ is given by:

$$\mathbf{D}=\frac{Eh^3}{12(1-\nu^2)}\begin{bmatrix}1 & \nu & 0\\ \nu & 1 & 0\\ 0 & 0 & \dfrac{(1-\nu)}{2}\end{bmatrix} \tag{2.45}$$

When going from a global coordinate system to a local one, we have the approximate solution $w(\xi, \eta)$ and the coefficients of the local stiffness matrix are given, respectively, by [12]:

$$w^{\mathrm{e}}(\xi, \eta) = \sum_{\mathrm{i}=1}^{n} u_{\mathrm{i}} N_{\mathrm{i}}^{\mathrm{e}}(\xi, \eta) \tag{2.46}$$

$$K_{\mathrm{i}j}^{\mathrm{e}} = \int_{\Omega^{\mathrm{e}}} \mathbf{B}_{\mathbf{i}}^{\mathbf{e}T} \mathbf{D} \mathbf{B}_{j}^{\mathrm{e}} \det(\mathbf{J})\, d\xi\, d\eta \tag{2.47}$$

Where the elementary stress-displacement vector $\mathbf{B}_{\mathrm{i}}^{\mathrm{e}}$ is composed of the second order derivatives of the local base functions $\{N_{\mathrm{i}}^{\mathrm{e}}(\xi, \eta)\}_{\mathrm{i}=1}^{n}$.

2.4.4 Numerical Analysis of Free Vibrations

The general equation of motion for a solid body is given by [14]:

$$\mathbf{M}\ddot{\mathbf{u}} + \mathbf{C}\dot{\mathbf{u}} + \mathbf{K}\mathbf{u} = \mathbf{f} \tag{2.48}$$

Where, $\mathbf{u}$ is the displacement vector, $\mathbf{M}$ is the Global Mass Matrix, $\mathbf{C}$ is the Global Damping Matrix, $\mathbf{K}$ is the Global Stiffness Matrix and $\mathbf{f}$ is the vector of external forces. Considering that there is no damping or external loads acting on the solid, the equation of motion in matrix form is reduced to [15]:

$$\mathbf{M}\ddot{\mathbf{u}} + \mathbf{K}\mathbf{u} = 0 \tag{2.49}$$

The general solution of Eq. (2.49) that describes the unforced and undamped vibrations of a solid is [13]:

$$\mathbf{u} = \overline{\mathbf{u}} \exp(\mathrm{i}\omega t) \tag{2.50}$$

In this equation, i is the imaginary unit, ω is the natural frequency, t is the time and $\overline{\mathbf{u}}$ is the eigenvector associated to ω. Replacing this solution in the Eq. (2.50), you get [15]:

$$\left(\mathbf{K} - \omega^2 \mathbf{M}\right) \overline{\mathbf{u}} = 0 \tag{2.51}$$

This equation represents a problem of eigenvalues, which allows to obtain the natural frequencies ω and their respective eigenvectors. The equation of eigenvalues has a non-trivial solution ($\mathbf{u} = 0$) when it is fulfilled that:

$$\det\left(\mathbf{K} - \omega^2\mathbf{M}\right) = 0 \tag{2.52}$$

This last equation is fulfilled for a discrete set of eigenvalues $\lambda_\mathrm{i} = \omega_\mathrm{i}^2$, with $\mathrm{i} = 1, 2, 3, ...$; where each λ_i has an associated vector $\mathbf{u_i}$, as shown in the following equation [8]:

$$\left(\mathbf{K} - \lambda_\mathrm{i}\mathbf{M}\right)\overline{\mathbf{u_i}} = 0 \tag{2.53}$$

For the case of a plate, the Global Stiffness Matrix $\mathbf{K}$ is obtained from Eq. (2.41) or (2.43) presented in the previous section, while the Global Mass Matrix $\mathbf{M}$ and its coefficients are given by [15]:

$$\mathbf{M} = \int_\Omega \rho h \mathbf{N}^\mathbf{T}\mathbf{N}\, d\Omega \tag{2.54}$$

$$M_{\mathrm{i}j} = \int_\Omega \rho h N_\mathrm{i} N_j\, d\Omega \tag{2.55}$$

Where ρ is the density of the material, h is the thickness of the plate, $\mathbf{N}$ is the vector that contains the basis functions and N_i is the i-th basis function that approximates the solution. Analogous to the Global Stiffness Matrix, you move from a global coordinate system to a local system as shown below:

$$M_{\mathrm{i}j}^\mathrm{e} = \int_{\Omega^\mathrm{e}} \rho h N_\mathrm{i}(\xi,\eta) N_j(\xi,\eta) \det(\mathbf{J})\, d\xi\, d\eta \tag{2.56}$$

Chapter 3

Methodology

The methodology of this thesis work is based on the implementation of the Geometry Independent Field approximaTion (GIFT) to study the static and dynamic response of thin plates, based on the Kirchhoff-Love Plate Theory (KLPT). To fulfill this, the following stages are established:

1. **Literature Review:** This first stage consists of carrying out a review of the bibliography related to the main concepts of this thesis work: Finite Element Method (FEM), IsoGeometric Analysis (IGA), Geometry Independent Field approximaTion (GIFT) and Kirchhoff-Love Plate Theory (KLPT).
2. **Characterization of Plates to study:** It consists in defining the geometry, its NURBS parameterization and material characteristics of the plates to be studied.
3. **GIFT Algorithm:** This stage consists in studying the algorithm developed in [3], which is programmed in C ++ language, and which allows to implement the GIFT to study 2-dimensional plate problems.
4. **Adaptation of the GIFT Code:** this stage consists in adapting the aforementioned code so that it is capable of generating different plate geometries.
5. **Application of the GIFT to the Plate Study:** this stage consists of extending the computer code, now available for Poisson's equation, for the study of plates, to obtain numerically the response, both static and dynamic, of each of the configurations studied in this report.
6. **Reference Solutions of the KLPT:** this stage consists in finding analytical solutions of vibrations and deflections, for those geometries where solutions exist. For complex geometries, reference solutions are the FEM solutions, obtained in ANSYS.
7. **Analysis and Comparison of Results:** This stage consists of comparing, for each one of the geometries studied, the static and dynamic response obtained by GIFT with the reference solutions.

The methodology is illustrated in Figure 3.1.

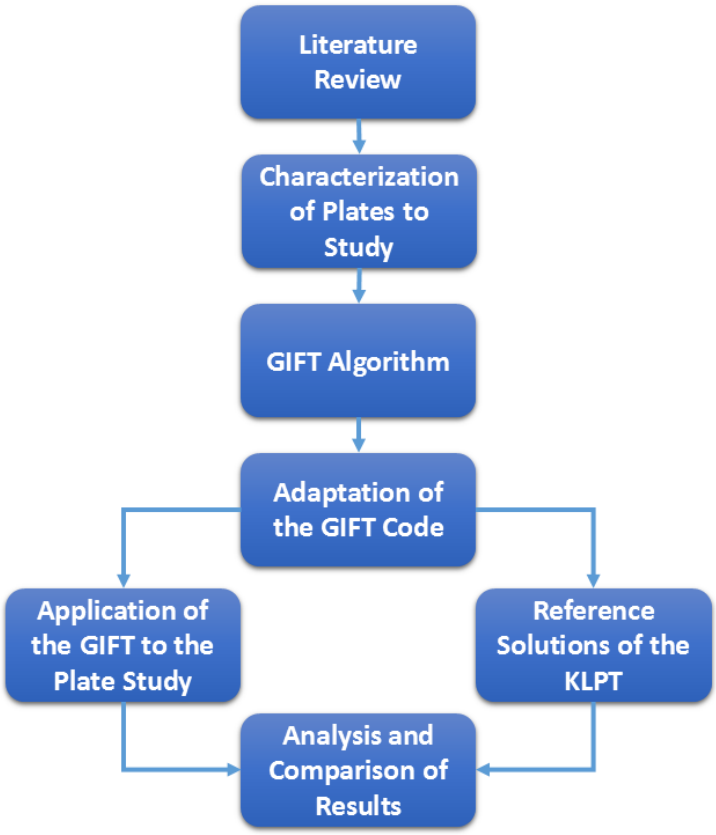

Figure 3.1: Methodology of this thesis work.

3.1 Resources

The resources needed to develop this thesis work are of the non-pecuniary type and are mainly related to the computational software used to develop it. These correspond to:

- Literature and additional bibliography.
- A computer code, programmed in C ++ language and generated with the Code::Blocks program, which is a free C++ IDE available for Windows, OS X and Linux operating system. This program also allows the implementation of GIFT.
- Mathematical software, such as Maple or Wolfram Mathematica, to solve the KLPT equations.
- For the data analysis and the Post-Processing of the results obtained with the GIFT code, the software Matlab® will be used, which is a not free numerical computing software, available for Windows, OS X and Linux operating system.

Chapter 4

Definition of the Problems

This thesis work seeks to demonstrate the applicability and performance of the GIFT method to solve plate vibration problems, an important area of solid mechanics. For this, 3 plates with different characteristics and complexities will be studied.

The first problem corresponds to the problem of a clamped circular plate subjected to a constant external load and whose geometry is generated from a single patch. The second problem is identical to the previous one, but with the difference that the circular geometry of the plate is generated with 2 patches. Finally, the last problem to study consists of a square plate clamped in all its boundaries and with a complicated shape hole in its center, whose geometry is generated by 8 patches.

The objectives of each of the problems are:

- **Problem 1:** The problem seeks to demonstrate the applicability and accuracy of the GIFT method to resolve a simple problem with an analytical solution known. The particular objective is to compare NURBS and B-Splines for the field approximation.
- **Problem 2:** Together with the aforementioned, this problem also seeks to demonstrate that in the framework of GIFT, the two-patch NURBS geometry can be paired with the one-patch B-Splines solution field, where the necessary continuity of the basis functions can be enforced directly on the solution basis without any coupling conditions between the geometry patches, unlike it is done in the standard IGA.
- **Problem 3:** This problem, in addition to the aforementioned, seeks to demonstrate the effectiveness of the GIFT method to solve problems with more complex and multi-patches geometries.

To compare the numerical results obtained with the GIFT method to the analytical ones, we will use the error measure given by the L^2-error, defined in the Eq. 4.1.

$$\|w - w^*\|_{L^2} = \left[\int_\Omega (w - w^*)^2\right]^{1/2} \tag{4.1}$$

Where w represented the numerical displacement obtained with the GIFT method and w^* is the displacement predicted by the theory.

4.1 Problem 1: Clamped Circular Plate with One-Patch Parameterization

The first problem consists in studying the symmetrical bending and free vibrations of a circular plate of radius a clamped around the edge with the geometry generated with a single patch.

The mechanical and physical properties of the plate material and the dimensions used to study the unforced deformations and vibrations of this plate are presented in Table 4.1 [16].

Table 4.1: Dimensions, mechanical and physical properties of the Circular Plate [16].

Property	Value	Unit of Measure
E	200	GPa
ν	0.3	-
ρ	7850	kg/m^3
a	0.5	m
h	0.01	m

4.1.1 Geometry

The knot vectors and the control points used to generate the geometry of a circular plate with $p = q = 2$ are given, respectively, by the Eq. (4.2) and Table 4.2 [17] [18].

$$\Xi = \{0, 0, 0, 1, 1, 1\} \qquad H = \{0, 0, 0, 1, 1, 1\} \tag{4.2}$$

Table 4.2: Control Points and respective weights to represent a circular plate of radius $a = 0.5[m]$ [17] [18].

i	1	2	3	4	5	6	7	8	9
x_i	$-\frac{\sqrt{2}}{4}$	$-\frac{\sqrt{2}}{2}$	$-\frac{\sqrt{2}}{4}$	0	0	0	$\frac{\sqrt{2}}{2}$	$\frac{\sqrt{2}}{2}$	$\frac{\sqrt{2}}{4}$
y_i	$\frac{\sqrt{2}}{4}$	0	$-\frac{\sqrt{2}}{4}$	$\frac{\sqrt{2}}{2}$	0	$-\frac{\sqrt{2}}{2}$	$\frac{\sqrt{2}}{2}$	0	$-\frac{\sqrt{2}}{4}$
w_i	1	$\frac{\sqrt{2}}{2}$	1	$\frac{\sqrt{2}}{2}$	1	$\frac{\sqrt{2}}{2}$	1	$\frac{\sqrt{2}}{2}$	1

These parameters allow one to generate a circle, as shown in Figure 4.1a, where one can see the geometry elements and the control points [17]. According to the GIFT method, in all following calculations, the original (coarse) geometry parameterization is used without any changes. However, in some study cases the solution is approximated by NURBS basis functions, derived from the geometry basis by p- and h- refinements. Such refined geometries are demonstrated in Figures 4.1b and 4.2 [19].

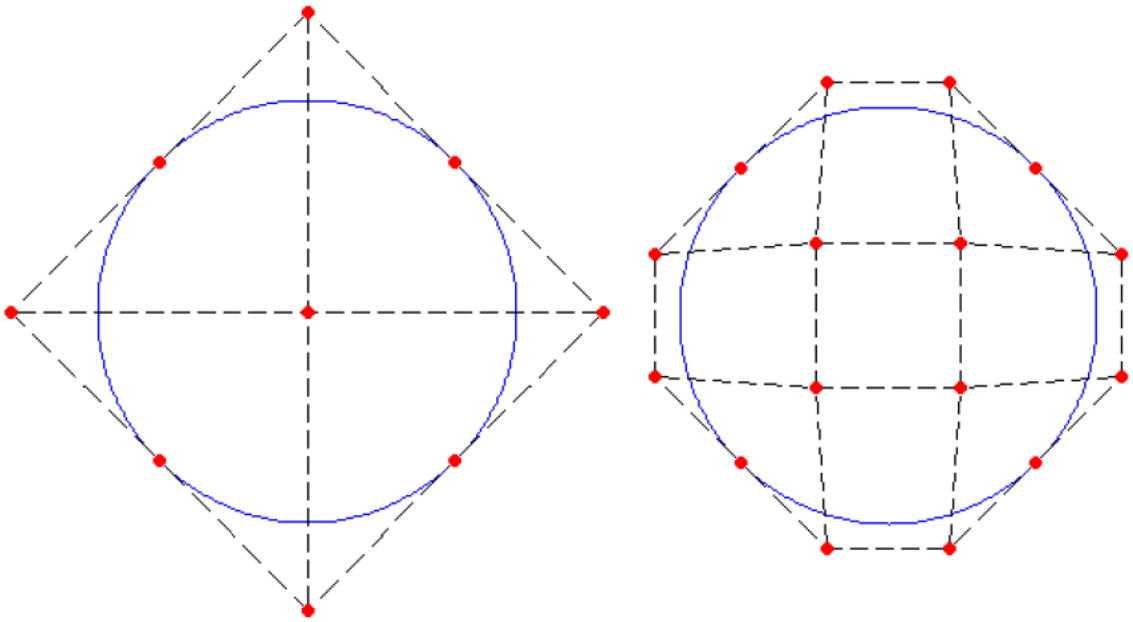

(a) $p = 2$ (b) $p = 3$.

Figure 4.1: Coarse mesh and control points of a circular plate for some polynomial degrees p [17].

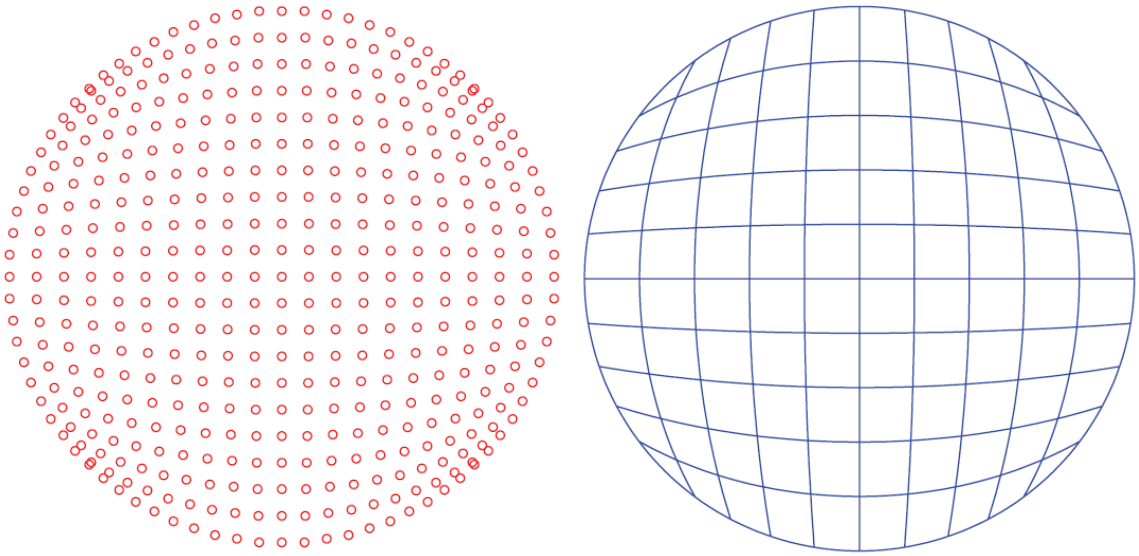

(a) Control Points. (b) Physical Mesh.

Figure 4.2: A 10×10 uniform meshed circular plate [19].

4.1.2 Analytical Solution for Symmetric Bending

The bending of a circular plate, using the KLPT, can be studied by analytical resolution of the governing equation, see Eq.(2.32), with the appropriate boundary conditions. In the case of bending, Eq.(2.32) can be re-written in cylindrical coordinates as:

$$D\nabla^2\nabla^2 w(r,\theta) = q \tag{4.3}$$

For the case of a circular plate subjected to a symmetric external load, $w(r,\theta) = w(r)$, so the equation is reduced to [20]:

$$\nabla^2\nabla^2 w(r) = \frac{1}{r}\frac{\mathrm{d}}{\mathrm{d}r}\left[r\frac{\mathrm{d}}{\mathrm{d}r}\left\{\frac{1}{r}\frac{\mathrm{d}}{\mathrm{d}r}\left(r\frac{\mathrm{d}w}{\mathrm{d}r}\right)\right\}\right] = \frac{q}{D} \tag{4.4}$$

In a particular case of a constant load, i.e. $q = -|q| = -q_o$, the solution of the ordinary differential equation (4.4) is obtained by direct integration, i.e:

$$w(r) = -\frac{q_o r^4}{64D} + C_1\ln(r) + C_2 r^2 + C_3 r^2\ln(r) + C_4 \tag{4.5}$$

Where the integration constants C_i, with $\mathrm{i} = 1, 2, 3, 4$; are determined by the boundary conditions. In the case of a complete circular plate, it is required that the deflections are finite at any point of it, so it must be imposed that $C_1 = 0$; since $\ln(r)$ tends to $-\infty$ in $r = 0$.

Considering the case of a clamped circular plate in the edge ($r = a$), the boundary conditions correspond to:

- $w(a) = 0$.
- $\dfrac{\partial w}{\partial r}(a) = 0$.

Imposing both boundary conditions, we obtain the equation that governs the behavior of a circular plate clamped in its radius a and holds under a constant and symmetrical external load [21]:

$$w(r) = -\frac{q_o}{64D}(r^2 - a^2)^2 \tag{4.6}$$

4.1.3 Analytical Solution for Free Vibrations

For free vibrations, the external load q is zero and the dynamic governing equation, see Eq. (2.33), is reduced to [10]:

$$D\nabla^2\nabla^2 w + \rho h\frac{\partial^2 w}{\partial t^2} = 0 \tag{4.7}$$

In what following, we quickly recall the derivation of the analytical solution given in [10].

Applying separation of variables to solve this partial differential equation, the solution has the form:

$$w(r,\theta,t) = W(r,\theta)T(t) \tag{4.8}$$

Substituting in the Eq. 4.7, the following two differential equations are obtained:

$$\frac{\mathrm{d}^2T}{\mathrm{d}t^2} + \omega^2 T = 0 \tag{4.9}$$

$$\nabla^4 W(r,\theta) - \lambda^4 W(r,\theta) = (\nabla^2 + \lambda^2)(\nabla^2 - \lambda^2)W(r,\theta) = 0 \tag{4.10}$$

Where,

$$\lambda^4 = w^2 \frac{\rho h}{D} \tag{4.11}$$

The Eq. 4.10 generates two partial differential equations:

$$\frac{\partial^2 W}{\partial r^2} + \frac{1}{r}\frac{\partial W}{\partial r} + \frac{1}{r^2}\frac{\partial^2 W}{\partial \theta^2} + \lambda^2 W = 0 \tag{4.12}$$

$$\frac{\partial^2 W}{\partial r^2} + \frac{1}{r}\frac{\partial W}{\partial r} + \frac{1}{r^2}\frac{\partial^2 W}{\partial \theta^2} - \lambda^2 W = 0 \tag{4.13}$$

Applying again the separation of variables, $W(r,\theta) = R(r)\Theta(\theta)$, the following ordinary differential equations are obtained:

$$\frac{\mathrm{d}^2\Theta}{\mathrm{d}\theta^2} + \alpha^2\Theta = 0 \tag{4.14}$$

$$r^2\frac{\mathrm{d}^2R}{\mathrm{d}r^2} + r\frac{\mathrm{d}R}{\mathrm{d}r} - \left(\pm\lambda^2 r^2 - \alpha^2\right)R = 0 \tag{4.15}$$

Where α^2 is a constant and an integer, so $\alpha = m = 0, 1, 2, 3, ...$ The solutions of the differential equations 4.14 and 4.15 are, respectively:

$$\Theta(\theta) = A\cos(m\theta) + B\sin(m\theta) \tag{4.16}$$

$$R(r) = C_1 J_m(\lambda r) + C_2 Y_m(\lambda r) + C_3 I_m(\lambda r) + C_4 K_m(\lambda r) \tag{4.17}$$

Where J_m and Y_m are the Bessel Functions of First and Second Kind, while I_m and K_m are the Modified Bessel Functions of First and Second Kind, respectively.

The general solution of spatial variables is given by [14]:

$$W(r,\theta) = \left[C_1 J_m(\lambda r) + C_2 Y_m(\lambda r) + C_3 I_m(\lambda r) + C_4 K_m(\lambda r)\right] \left\{A\cos(m\theta) + B\sin(m\theta)\right\} \tag{4.18}$$

Considering that the solutions of $W(r,\theta)$ must be finite in any part of the circular plate, it must be imposed that C_2 and C_4 are equal to 0 because the Bessel functions Y_m and K_m tend to infinity at $r = 0$. In addition, for the case where the plate is embedded in the edge $r = a$, the boundary conditions are the following:

$$W(a,\theta) = 0 \tag{4.19}$$

$$\frac{\mathrm{d}W}{\mathrm{d}r}(a,\theta) = 0 \tag{4.20}$$

By imposing the boundary condition given by the Eq. 4.20, you get [11]:

$$J_m(\lambda a) I_{m+1}(\lambda a) + J_{m+1}(\lambda a) I_m(\lambda a) = 0 \tag{4.21}$$

This corresponds to the characteristic equation of a clamped circular plate, whose roots allow to obtain the natural frequencies of the different vibration modes of the plate; as follows:

$$\lambda_{mn} = \omega_{mn}\sqrt{\frac{\rho h}{D}} \tag{4.22}$$

Using this in the Eq. (4.18), the spatial equation is given by:

$$W_{mn}(r,\theta) = \left[J_m(\lambda_{mn} r) I_m(\lambda_{mn} a) - J_m(\lambda_{mn} a) I_m(\lambda_{mn} r)\right] \begin{Bmatrix}\cos(m\theta)\\ \sin(m\theta)\end{Bmatrix} \tag{4.23}$$

On the other hand, the solution of the Eq. 4.9 is:

$$T_{mn}(t) = D^1_{mn}\cos(\omega_{mn} t) + E^1_{mn}\cos(\omega_{mn} t) \tag{4.24}$$

The general equation for free vibrations of a clamped circular plate is given by [10]:

$$w(r,\theta,t) = \sum_{m=0}^{\infty}\sum_{n=0}^{\infty}\{[J_m(\lambda_{mn}r)I_m(\lambda_{mn}a) - J_m(\lambda_{mn}a)I_m(\lambda_{mn}r)]\cos(m\theta)\}\left(A^1_{mn}\cos(\omega_{mn}t) + A^2_{mn}\sin(\omega_{mn}t)\right)$$
$$+\sum_{m=0}^{\infty}\sum_{n=0}^{\infty}\{[J_m(\lambda_{mn}r)I_m(\lambda_{mn}a) - J_m(\lambda_{mn}a)I_m(\lambda_{mn}r)]\sin(m\theta)\}\left(A^3_{mn}\cos(\omega_{mn}t) + A^4_{mn}\sin(\omega_{mn}t)\right) \tag{4.25}$$

Where the constants A^{i}_{mn}, with $\mathrm{i} = 1, 2, 3, 4$, are determined by the initial conditions.

4.2 Problem 2: Clamped Circular Plate with Two-Patch Parameterization

The second problem consists only in the symmetrical bending of a circular plate embedded around the edge, parameterized by two patches in three different ways, in which the divisions between the patches can be classified as regular or irregular.

The mechanical and physical properties of the plate material and the dimensions used to study the bending problem of this plate are the same that it was presented in Table 4.1 for the first problem.

4.2.1 Geometry

In this case, the division of the circle can be regular or irregular. The regular division implies the division of the circle into two equal halves, while the irregular division generates two halves of a circle that are not equal to each other.

Regular Division with 2 Patches

The knot vectors of each of the patches are given, respectively, by the Eq. 4.26 and 4.27, and the control points are tabulated in Table 4.3.

- **Patch 1: Left Half of a Circle.**

$$\Xi = \left\{0, 0, 0, \frac{1}{2}, \frac{1}{2}, \frac{1}{2}\right\} \qquad H = \left\{0, 0, 0, \frac{1}{4}, \frac{1}{2}, \frac{3}{4}, 1, 1, 1\right\} \tag{4.26}$$

- **Patch 2: Right Half of a Circle.**

$$\Xi = \left\{\frac{1}{2}, \frac{1}{2}, \frac{1}{2}, 1, 1, 1\right\} \qquad H = \left\{0, 0, 0, \frac{1}{4}, \frac{1}{2}, \frac{3}{4}, 1, 1, 1\right\} \tag{4.27}$$

These parameters allow generating a circle divided into two equal parts, as shown in Figure 4.3, where one can see the coarse mesh and the control points of each of the parts. In addition, in Figure 4.3, one can see the distribution of control points on the surface of the circle and the physical mesh generated for a certain refinement of the geometry. Though note, that in all numerical calculations, the original coarse geometry is used.

Table 4.3: Control Points of each of the semicircles.

Left Half Circle				Right Half Circle			
i	x_i	y_i	w_i	i	x_i	y_i	w_i
1	-0.35355	0.35355	1	1	0	0.5	0.85355
2	-0.42099	0.28612	0.92678	2	0	0.375	0.85355
3	-0.5	0.10355	0.85355	3	0	0.125	0.85355
4	-0.5	-0.10355	0.85355	4	0	-0.125	0.85355
5	-0.42099	-0.28612	0.92678	5	0	-0.375	0.85355
6	-0.35355	-0.35355	1	6	0	-0.5	0.85355
7	-0.20711	0.5	0.85355	7	0.20711	0.5	0.85355
8	-0.22855	0.375	0.85355	8	0.22855	0.375	0.85355
9	-0.25	0.125	0.85355	9	0.25	0.125	0.85355
10	-0.25	-0.125	0.85355	10	0.25	-0.125	0.85355
11	-0.22855	-0.375	0.85355	11	0.22855	-0.375	0.85355
12	-0.20711	-0.5	0.85355	12	0.20711	-0.5	0.85355
13	0	0.5	0.85355	13	0.35355	0.35355	1
14	0	0.375	0.85355	14	0.42099	0.28612	0.92678
15	0	0.125	0.85355	15	0.5	0.10355	0.85355
16	0	-0.125	0.85355	16	0.5	-0.10355	0.85355
17	0	-0.375	0.85355	17	0.42099	-0.28612	0.92678
18	0	-0.5	0.85355	18	0.35355	-0.35355	1

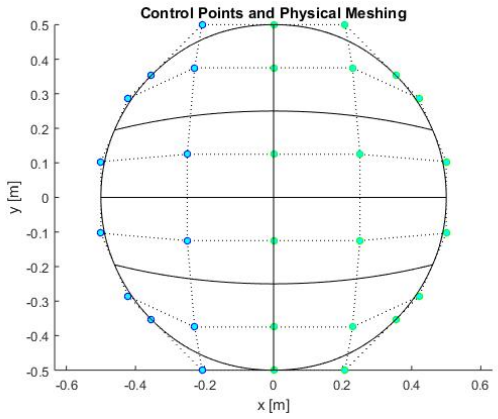

(a) Coarse Geometry.

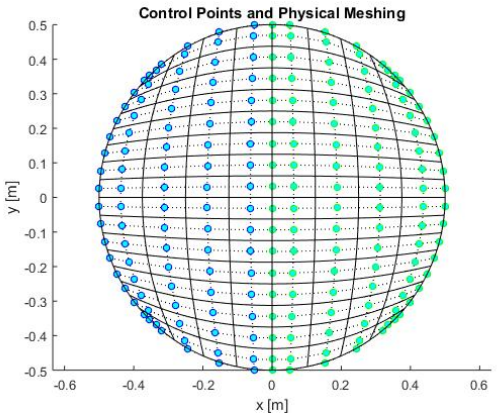

(b) Refined Geometry.

Figure 4.3: Coarse and refined distribution of the 2 generating patches of a circle together with their respective physical mesh.

Irregular Division with 2 Patches

In this section, two ways of generating the circular geometry of 2 patches with an irregular division are described: the $\succ$-shape and the $\wr$-shape.

The knot vectors used to generate each of the parts of the aforementioned cases correspond to the same ones already used to construct the circular geometry with a regular division, that

is, those given by the Eq. (4.26) and (4.27). The control points of each of the parts for the $\succ$-shape and the $\wr$-shape parameterizations, are given, respectively, by the Tables 4.4 and 4.5.

In the Figures 4.4 and 4.5, the distributions of the control points are shown in a coarse and refined way for each of the cases mentioned above. Note, that in the calculations, only the coarse geometry is used.

Table 4.4: Control Points of each of the semicircles of radius $a = 0.5[m]$ for the $\succ$-shape parameterization.

	Left Half Circle				Right Half Circle		
i	x_i	y_i	w_i	i	x_i	y_i	w_i
1	-0.35355	0.35355	1	1	0	0.5	0.85355
2	-0.42099	0.28612	0.92678	2	-0.15	0.25	0.85355
3	-0.5	0.10355	0.85355	3	0	0	0.85355
4	-0.5	-0.10355	0.85355	4	0	0	0.85355
5	-0.42099	-0.28612	0.92678	5	-0.15	-0.25	0.85355
6	-0.35355	-0.35355	1	6	0	-0.5	0.85355
7	-0.20711	0.5	0.85355	7	0.20711	0.5	0.85355
8	-0.22855	0.375	0.85355	8	0.22855	0.375	0.85355
9	-0.25	0.125	0.85355	9	0.25	0.125	0.85355
10	-0.25	-0.125	0.85355	10	0.25	-0.125	0.85355
11	-0.22855	-0.375	0.85355	11	0.22855	-0.375	0.85355
12	-0.20711	-0.5	0.85355	12	0.20711	-0.5	0.85355
13	0	0.5	0.85355	13	0.35355	0.35355	1
14	-0.15	0.25	0.85355	14	0.42099	0.28612	0.92678
15	0	0	0.85355	15	0.5	0.10355	0.85355
16	0	0	0.85355	16	0.5	-0.10355	0.85355
17	-0.15	-0.25	0.85355	17	0.42099	-0.28612	0.92678
18	0	-0.5	0.85355	18	0.35355	-0.35355	1

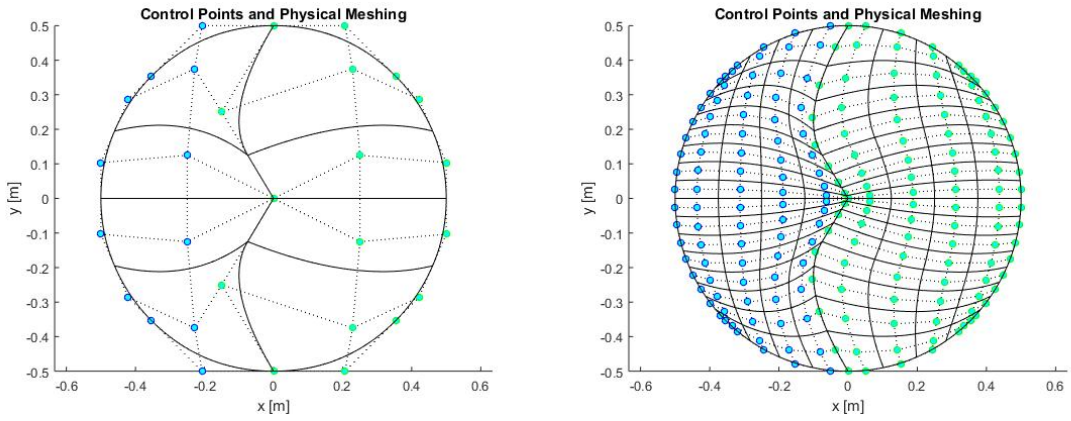

(a) Coarse Geometry.

(b) Refined Geometry.

Figure 4.4: Coarse and refined geometry with the $\succ$-shape parameterization.

Table 4.5: Control Points of each of the semicircles of radius $a = 0.5[m]$ for the ɾ-shape parameterization.

Left Half Circle				Right Half Circle			
i	x_i	y_i	w_i	i	x_i	y_i	w_i
1	-0.35355	0.35355	1	1	0	0.5	0.85355
2	-0.42099	0.28612	0.92678	2	0.15	0.25	0.85355
3	-0.5	0.10355	0.85355	3	0	0	0.85355
4	-0.5	-0.10355	0.85355	4	0	0	0.85355
5	-0.42099	-0.28612	0.92678	5	-0.15	-0.25	0.85355
6	-0.35355	-0.35355	1	6	0	-0.5	0.85355
7	-0.20711	0.5	0.85355	7	0.20711	0.5	0.85355
8	-0.22855	0.375	0.85355	8	0.22855	0.375	0.85355
9	-0.25	0.125	0.85355	9	0.25	0.125	0.85355
10	-0.25	-0.125	0.85355	10	0.25	-0.125	0.85355
11	-0.22855	-0.375	0.85355	11	0.22855	-0.375	0.85355
12	-0.20711	-0.5	0.85355	12	0.20711	-0.5	0.85355
13	0	0.5	0.85355	13	0.35355	0.35355	1
14	0.15	0.25	0.85355	14	0.42099	0.28612	0.92678
15	0	0	0.85355	15	0.5	0.10355	0.85355
16	0	0	0.85355	16	0.5	-0.10355	0.85355
17	-0.15	-0.25	0.85355	17	0.42099	-0.28612	0.92678
18	0	-0.5	0.85355	18	0.35355	-0.35355	1

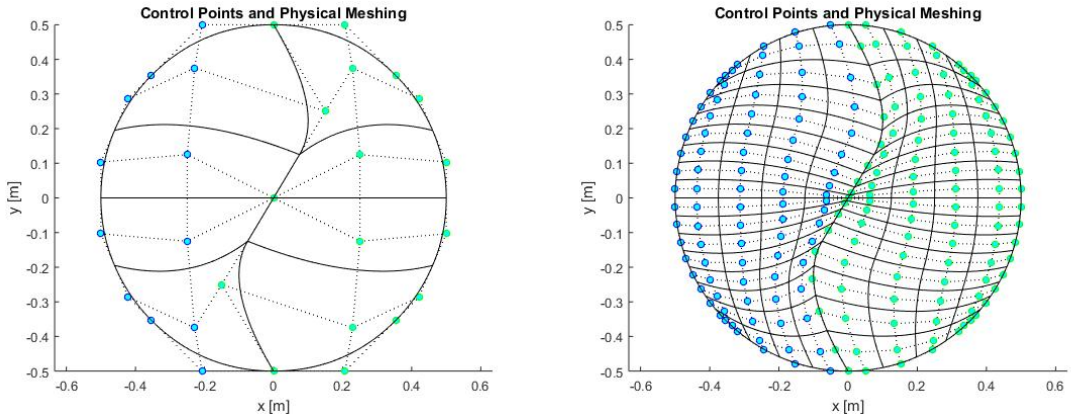

(a) Coarse Geometry.

(b) Refined Geometry.

Figure 4.5: Coarse and refined geometry with the ɾ-shape parameterization.

4.3 Problem 3: Clamped Square Plate with a cut-out of Complicated Shape, composed by 8 Patches

The last problem of this work corresponds to studying the deflection and free vibrations of a square plate clamped at all its edges and that has a hole of a complicated shape. For this problem, the results for the bending are compared with the ANSYS FEM model and for the vibrations it is compared with the results obtained in [8] and [22]:

4.3.1 Geometry

The dimensions and the 8 patches that make up the square plate with a heart-shaped hole can be seen in Figure 4.6. The physical and mechanical properties of the plate material are shown in Table 4.6.

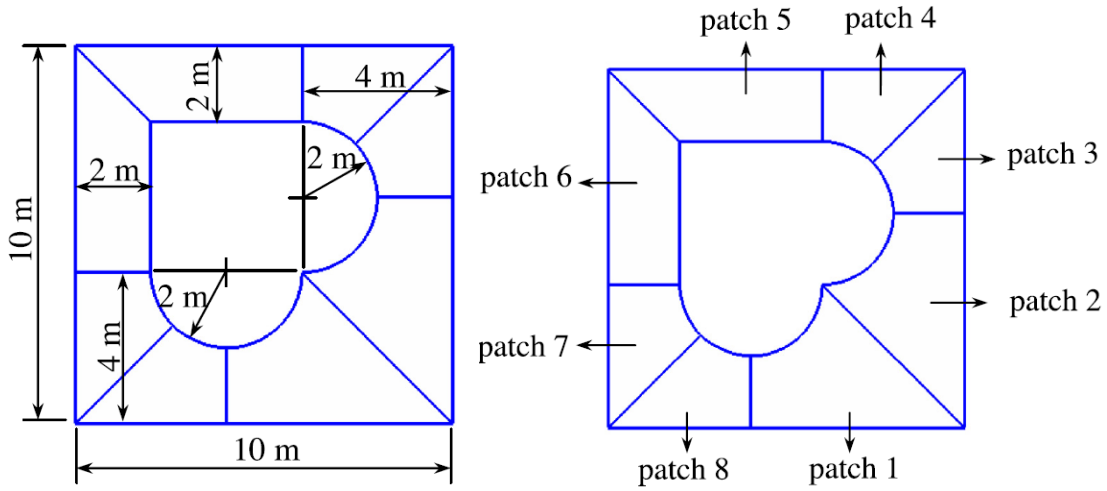

(a) Dimensions of the Plate.

(b) 8 Patches of the Geometry.

Figure 4.6: Dimensions and the 8 patches of the square plate with a complicated shaped hole [8].

Table 4.6: Physical and mechanical properties of the Square Plate with a Complicated Hole.

Property	Value	Units of Measurement
E	200	GPa
ν	0.3	-
ρ	8000	kg/m^3
h	0.05	m

The knot vectors and the order of the polynomials of the NURBS basis functions used for each of the patches are presented in Table 4.7; while the control points together with the respective weights of each of the patches are tabulated in Table 4.8.

Table 4.7: Degree of the polynomials and knot vectors of the 8 patches of the geometry of the plate [8].

Patch	ξ	η
1	$p = 2$ $\Xi = \{0, 0, 0, \frac{1}{8}, \frac{1}{8}, \frac{1}{8}\}$	$q = 1$ $H = \{0, 0, 1, 1\}$
2	$p = 2$ $\Xi = \{\frac{1}{8}, \frac{1}{8}, \frac{1}{8}, \frac{2}{8}, \frac{2}{8}, \frac{2}{8}\}$	$q = 1$ $H = \{0, 0, 1, 1\}$
3	$p = 2$ $\Xi = \{\frac{2}{8}, \frac{2}{8}, \frac{2}{8}, \frac{3}{8}, \frac{3}{8}, \frac{3}{8}\}$	$q = 1$ $H = \{0, 0, 1, 1\}$
4	$p = 2$ $\Xi = \{\frac{3}{8}, \frac{3}{8}, \frac{3}{8}, \frac{4}{8}, \frac{4}{8}, \frac{4}{8}\}$	$q = 1$ $H = \{0, 0, 1, 1\}$
5	$p = 1$ $\Xi = \{\frac{4}{8}, \frac{4}{8}, \frac{5}{8}, \frac{5}{8}\}$	$q = 1$ $H = \{0, 0, 1, 1\}$
6	$p = 1$ $\Xi = \{\frac{5}{8}, \frac{5}{8}, \frac{6}{8}, \frac{6}{8}\}$	$q = 1$ $H = \{0, 0, 1, 1\}$
7	$p = 2$ $\Xi = \{\frac{6}{8}, \frac{6}{8}, \frac{6}{8}, \frac{7}{8}, \frac{7}{8}, \frac{7}{8}\}$	$q = 1$ $H = \{0, 0, 1, 1\}$
8	$p = 2$ $\Xi = [\frac{7}{8}, \frac{7}{8}, \frac{7}{8}, 1, 1, 1]$	$q = 1$ $H = \{0, 0, 1, 1\}$

These parameters allow one to generate a square plate with a heart shaped hole, as shown in Figure 4.7, where one can see the coarse meshing and the control points for NURBS of third and forth degrees and different levels of $h-$refinement [23].

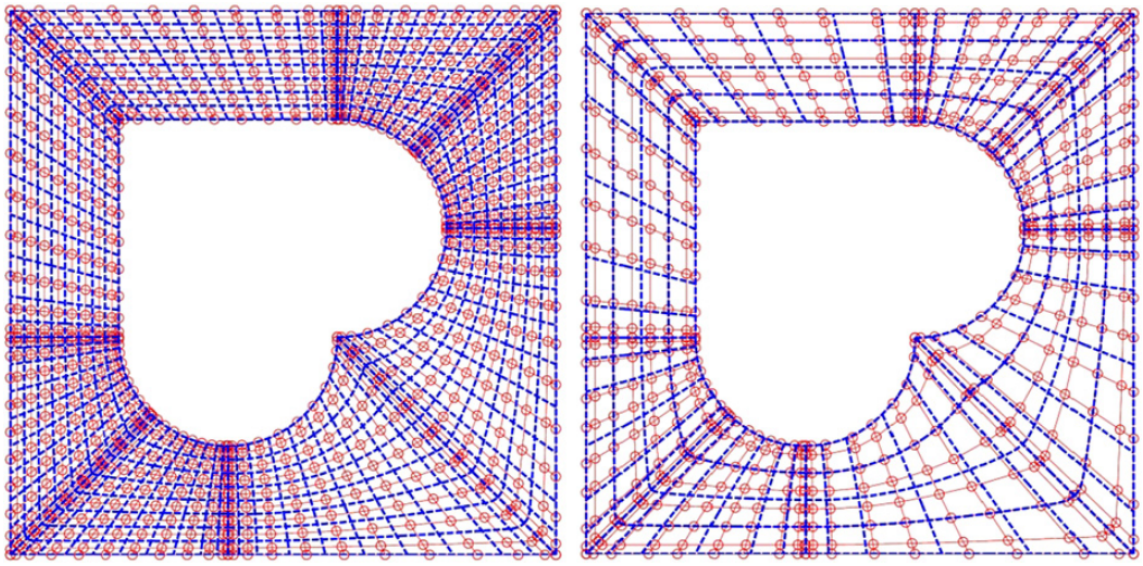

(a) Quadratic NURBS functions. (b) Cubic NURBS functions.

Figure 4.7: Control mesh and physical mesh of the plate with a hole of complicated shape. (a) Quadratic NURBS basis functions with 880 control points and 640 elements. (b) Cubic NURBS basis functions with 576 control points and 192 elements [23].

Table 4.8: Control Points of the 8 patches of the square plate [8].

Patch	i	j	x_{i}	y_{i}	w_{i}
1	1	1	4	0	1
	1	2	4	2	1
	2	1	7	0	1
	2	2	6	2	$\sqrt{2}/2$
	3	1	10	0	1
	3	2	6	4	1
2	1	1	10	0	1
	1	2	6	4	1
	2	1	10	3	1
	2	2	8	4	$\sqrt{2}/2$
	3	1	10	6	1
	3	2	8	6	1
3	1	1	10	6	1
	1	2	8	6	1
	2	1	10	8	1
	2	2	8	$6 + 2\tan\left(\frac{\pi}{8}\right)$	$\cos\left(\frac{\pi}{8}\right)$
	3	1	10	10	1
	3	2	$6 + \sqrt{2}$	$6 + \sqrt{2}$	1
4	1	1	10	10	1
	1	2	$6 + \sqrt{2}$	$6 + \sqrt{2}$	1
	2	1	8	10	1
	2	2	$6 + 2\tan\left(\frac{\pi}{8}\right)$	8	$\cos\left(\frac{\pi}{8}\right)$
	3	1	6	10	1
	3	2	6	8	1
5	1	1	6	10	1
	1	2	6	8	1
	2	1	0	10	1
	2	2	2	8	1
6	1	1	0	10	1
	1	2	2	8	1
	2	1	0	4	1
	2	2	2	4	1
7	1	1	0	4	1
	1	2	2	4	1
	2	1	0	2	1
	2	2	2	$4 - 2\tan\left(\frac{\pi}{8}\right)$	$\cos\left(\frac{\pi}{8}\right)$
	3	1	0	0	1
	3	2	$4 - \sqrt{2}$	$4 - \sqrt{2}$	1
8	1	1	0	0	1
	1	2	$4 - \sqrt{2}$	$4 - \sqrt{2}$	1
	2	1	2	0	1
	2	2	$4 - 2\tan\left(\frac{\pi}{8}\right)$	2	$\cos\left(\frac{\pi}{8}\right)$
	3	1	4	0	1
	3	2	4	2	1

Chapter 5

Results

In this section the results obtained in numerical and analytical form for each of the problems of this thesis work are presented.

5.1 Problem 1: Clamped Circular Plate with One-Patch Parameterization.

5.1.1 Solution Bases

To study this plate, the geometry was generated using NURBS basis functions given in Table 4.2 and Eq. (4.2), and the corresponding result is shown in Figure 5.1. To approximate the solution, both NURBS and B-Splines functions were used. In order to construct the solution bases, the same knot vectors as for the geometry parameterization are first selected:

$$\Sigma = \{0, 0, 0, 1, 1, 1\}, \;\; \Pi = \{0, 0, 0, 1, 1, 1\}. \tag{5.1}$$

Then, the NURBS basis of degree $p = q = 2$ is chosen to be the same as in the geometry parameterization given in Table 4.2. The degree of the NURBS basis is subsequently raised using the algorithm of degree elevation to $p = q = 3, 4, 5$. In what follows, the corresponding bases are denoted as $N_{p,q}$. The bases are then refined using the algorithm of knot insertion.

The B-Spline solution basis of degree $p = q = 2$ is constructed on knot vectors, see Eq. (5.1), by setting all weights to be equal to 1. The degree of the B-Splines basis is subsequently raised using the algorithm of degree elevation to $p = q = 3, 4, 5$. In what follows, the corresponding bases are denoted as $B_{p,q}$. Then the h-refinement by knot insertion is performed.

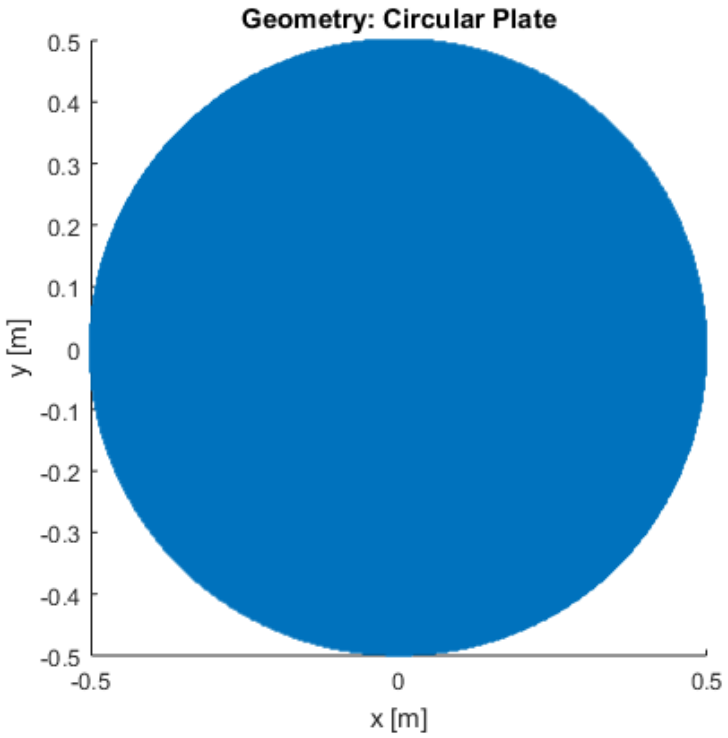

Figure 5.1: Geometry of a circular plate of radius $a = 0.5[m]$ generated with NURBS functions.

5.1.2 Bending Symmetric Problem

Considering the case of the clamped plate subjected to a symmetrical and constant external load of $q = q_o = 1[kPa]$, it follows from the analytical solution, see Eq. (4.6), that the maximum deflection is reached at the center $r = 0$ and has a theoretical value of [20]:

$$w_{max} = -\frac{q_o a^4}{64D} = -0.0533[mm] \tag{5.2}$$

For this case, in Figures 5.2 and 5.3, the deformed shape is shown, obtained both theoretically and numerically. The numerical results, shown graphically in Figure 5.3, were obtained by using basis $N_{5,5}$ and 1024 elements.

Figure 5.4 shows the comparison between the theoretical displacement and the numerical solution obtained using $N_{5,5}$ and 1024 elements.

Figure 5.5 shows the convergence curves obtained for the different degrees of polynomials and NURBS and B-Splines basis functions for the solution approximation, namely $N_{2,2}$, $B_{2,2}$, $N_{3,3}$, $B_{3,3}$, $N_{4,4}$, $B_{4,4}$, $N_{5,5}$ and $B_{5,5}$.

Table 5.1 shows the slopes for the different cases of convergence studied and presented graphically in Figure 5.5.

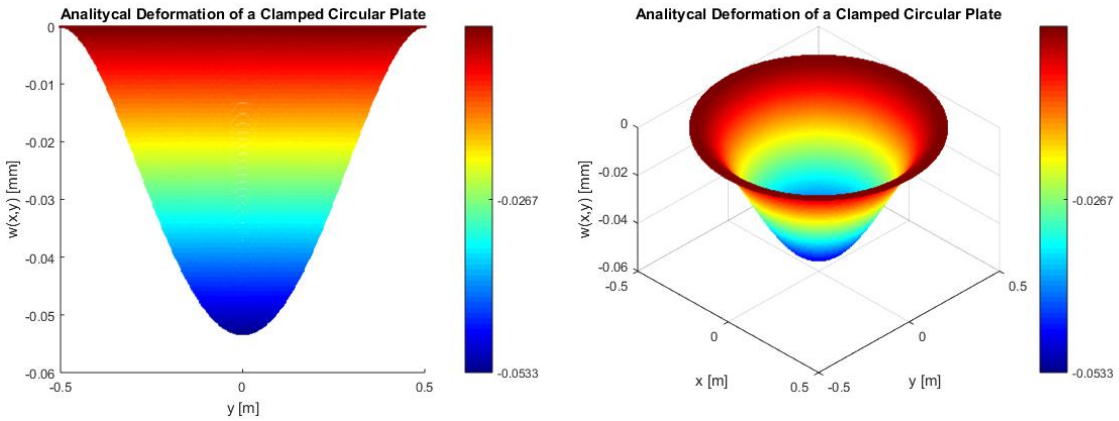

(a) Front view. (b) 3-D view.

Figure 5.2: Theoretical transverse displacement of a clamped circular plate.

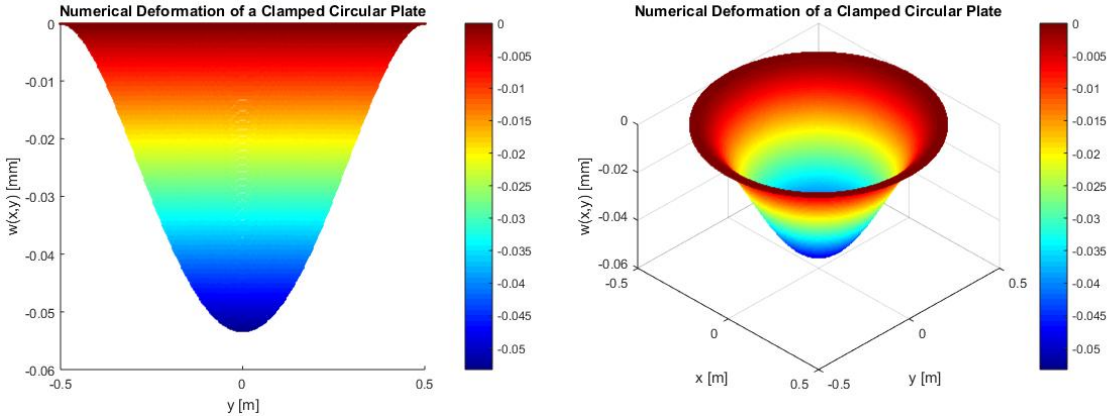

(a) Front view. (b) 3-D view

Figure 5.3: Numerical transverse displacement of a clamped circular plate.

Table 5.1: Convergence rates for each approximation function of the solution.

(p, q)	Theory [24] [25] [26]	NURBS	B-Splines
(2,2)	3	2.2	2.2
(3,3)	4	5.11	5.15
(4,4)	5	5.96	6
(5,5)	6	7.48	7.53

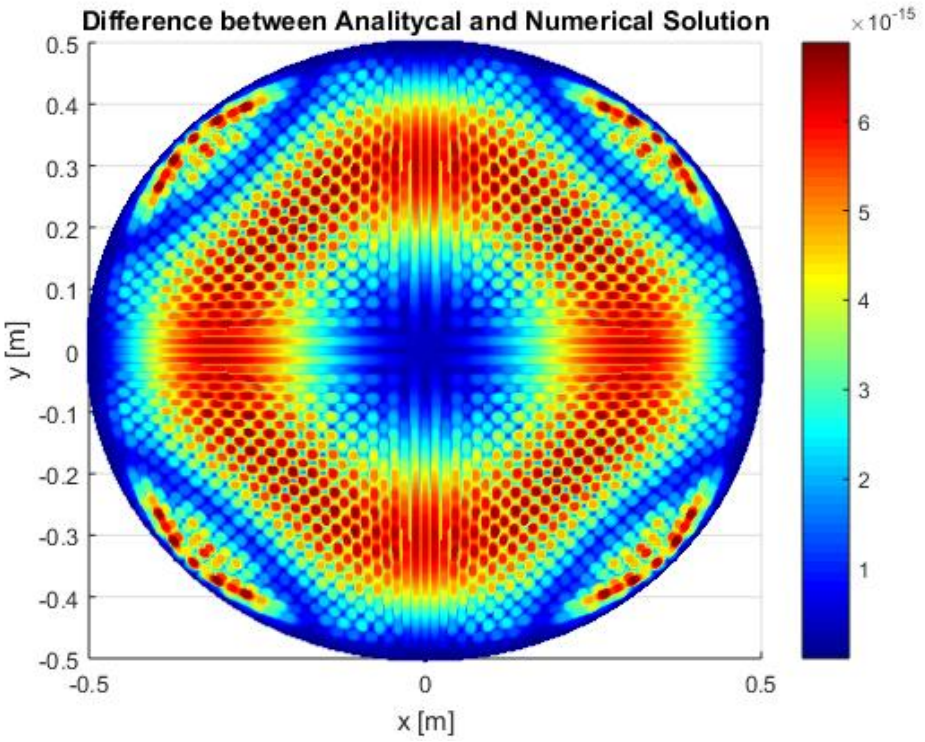

Figure 5.4: Absolute difference between the theoretical displacement and the numerical solution obtained using $N_{5,5}$ and 1024 elements.

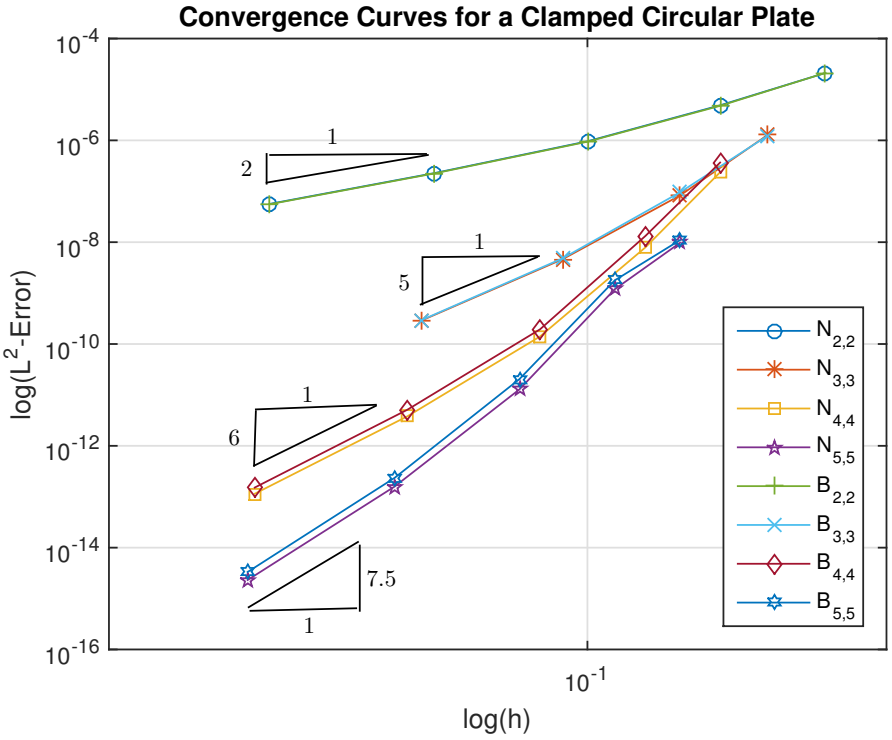

Figure 5.5: Convergence curves of the different cases studied for a clamped circular plate.

5.1.3 Free Vibrations Problem

The natural dimensionless frequencies β_{mn} are given analytically by [16]:

$$\beta_{mn} = \lambda_{mn} a = \left(\omega_{mn}^2 a^4 \frac{\rho h}{D} \right)^{1/4} \tag{5.3}$$

In the Tables 5.2 and 5.3, the theoretical values of the natural dimensionless frequencies β_{mn}, from [10], are listed together with the corresponding numerical results, obtained using $B_{2,2}$ and $B_{5,5}$ with and 1024 elements, respectively.

In Tables 5.4 and 5.5 the results obtained with NURBS bases, i.e. $N_{2,2}$ and $N_{5,5}$ with 1024 elements are listed.

Table 5.2: Dimensionless Natural Frequencies β_{mn} of a Clamped Circular Plate using basis $B_{2,2}$ with 1024 elements.

m Nodal Diameters	Results	n Nodal Circles			
		0	1	2	3
0	Exact	3.196217	4.6109	5.905929	7.144228
	Numerical	3.198069	4.616915	5.911821	7.166465
	Error (%)	$5.79{\cdot}10^{-2}$	$1.3{\cdot}10^{-1}$	$9.98{\cdot}10^{-2}$	$3.11{\cdot}10^{-1}$
1	Exact	6.306425	7.798718	9.196739	10.53613
	Numerical	6.321035	7.826841	9.221098	10.60179
	Error (%)	$2.32{\cdot}10^{-1}$	$3.61{\cdot}10^{-1}$	$2.65{\cdot}10^{-1}$	$6.23{\cdot}10^{-1}$
2	Exact	9.439492	10.9581	12.40202	13.79493
	Numerical	9.487346	11.03392	12.46293	13.9296
	Error (%)	$1.82{\cdot}10^{-1}$	$6.92{\cdot}10^{-1}$	$4.91{\cdot}10^{-1}$	$9.76{\cdot}10^{-1}$
3	Exact	12.577108	14.10886	15.57915	17.005
	Numerical	12.55427	13.9296	15.45366	17.07051
	Error (%)	$1.82{\cdot}10^{-1}$	1.27	$8.05{\cdot}10^{-1}$	$3.85{\cdot}10^{-1}$
4	Exact	15.71639	17.25601	18.74513	20.19208
	Numerical	15.70346	17.23816	18.73814	20.17515
	Error (%)	$8.23{\cdot}10^{-2}$	$1.03{\cdot}10^{-1}$	$3.73{\cdot}10^{-2}$	$8.38{\cdot}10^{-2}$

Table 5.3: Dimensionless Natural Frequencies β_{mn} of a Clamped Circular Plate using basis $B_{5,5}$ with 1024 elements.

m Nodal Diameters	Results	n Nodal Circles			
		0	1	2	3
0	Exact	3.196217	4.6109	5.905929	7.144228
	Numerical	3.196221	4.6109	5.905678	7.143531
	Error (%)	$1.25{\cdot}10^{-4}$	0	$4.25{\cdot}10^{-3}$	$9.76{\cdot}10^{-3}$
1	Exact	6.306425	7.798718	9.196739	10.53613
	Numerical	6.306437	7.799274	9.196883	10.53667
	Error (%)	$1.9{\cdot}10^{-4}$	$7.13{\cdot}10^{-3}$	$1.57{\cdot}10^{-3}$	$5.13{\cdot}10^{-3}$
2	Exact	9.439492	10.9581	12.40202	13.79493
	Numerical	9.439499	10.95807	12.40222	13.79506
	Error (%)	$7.42{\cdot}10^{-5}$	$2.74{\cdot}10^{-4}$	$1.61{\cdot}10^{-3}$	$9.42{\cdot}10^{-4}$
3	Exact	12.577108	14.10886	15.57915	17.005
	Numerical	12.57713	14.10883	15.57949	17.0053
	Error (%)	$1.75{\cdot}10^{-4}$	$1.63{\cdot}10^{-3}$	$2.18{\cdot}10^{-3}$	$1.76{\cdot}10^{-3}$
4	Exact	15.71639	17.25601	18.74513	20.19208
	Numerical	15.71644	17.25573	18.74397	20.19234
	Error (%)	$3.18{\cdot}10^{-4}$	$1.62{\cdot}10^{-3}$	$6.19{\cdot}10^{-3}$	$1.29{\cdot}10^{-3}$

Table 5.4: Dimensionless Natural Frequencies β_{mn} of a Clamped Circular Plate obtained using basis $N_{2,2}$ with 1024 elements.

m Nodal Diameters	Results	n Nodal Circles			
		0	1	2	3
0	Exact	3.196217	4.6109	5.905929	7.144228
	Numerical	3.198081	4.616927	5.911779	7.166362
	Error (%)	$5.83{\cdot}10^{-2}$	$1.31{\cdot}10^{-1}$	$9.91{\cdot}10^{-2}$	$3.1{\cdot}10^{-1}$
1	Exact	6.306425	7.798718	9.196739	10.53613
	Numerical	6.32111	7.82693	9.221159	10.60182
	Error (%)	$2.33{\cdot}10^{-1}$	$3.62{\cdot}10^{-1}$	$2.66{\cdot}10^{-1}$	$6.23{\cdot}10^{-1}$
2	Exact	9.439492	10.9581	12.40202	13.79493
	Numerical	9.487488	11.03408	12.46293	13.92975
	Error (%)	$5.08{\cdot}10^{-1}$	$6.93{\cdot}10^{-1}$	$4.91{\cdot}10^{-1}$	$9.77{\cdot}10^{-1}$
3	Exact	12.577108	14.10886	15.57915	17.005
	Numerical	12.55442	13.92975	15.45366	17.07051
	Error (%)	$1.82{\cdot}10^{-1}$	1.27	$8.05{\cdot}10^{-1}$	$3.85{\cdot}10^{-1}$
4	Exact	15.71639	17.25601	18.74513	20.19208
	Numerical	15.70346	17.23816	18.73814	20.17515
	Error (%)	$8.23{\cdot}10^{-2}$	$1.03{\cdot}10^{-1}$	$3.73{\cdot}10^{-2}$	$8.38{\cdot}10^{-2}$

Table 5.5: Dimensionless Natural Frequencies β_{mn} of a Clamped Circular Plate obtained using basis $N_{5,5}$ with 1024 elements.

m Nodal Diameters	Results	n Nodal Circles			
		0	1	2	3
0	Exact	3.196217	4.6109	5.905929	7.144228
	Numerical	3.196221	4.6109	5.905678	7.143531
	Error (%)	$1.25{\cdot}10^{-4}$	0	$4.25{\cdot}10^{-3}$	$9.76{\cdot}10^{-3}$
1	Exact	6.306425	7.798718	9.196739	10.53613
	Numerical	6.306437	7.799274	9.196883	10.53667
	Error (%)	$1.9{\cdot}10^{-4}$	$7.13{\cdot}10^{-3}$	$1.57{\cdot}10^{-3}$	$5.13{\cdot}10^{-3}$
2	Exact	9.439492	10.9581	12.40202	13.79493
	Numerical	9.439499	10.95807	12.40222	13.79506
	Error (%)	$7.42{\cdot}10^{-5}$	$2.74{\cdot}10^{-4}$	$1.61{\cdot}10^{-3}$	$9.42{\cdot}10^{-4}$
3	Exact	12.577108	14.10886	15.57915	17.005
	Numerical	12.57713	14.10883	15.57949	17.0053
	Error (%)	$1.75{\cdot}10^{-4}$	$1.63{\cdot}10^{-3}$	$2.18{\cdot}10^{-3}$	$1.76{\cdot}10^{-3}$
4	Exact	15.71639	17.25601	18.74513	20.19208
	Numerical	15.71644	17.25573	18.74397	20.19234
	Error (%)	$3.18{\cdot}10^{-4}$	$1.62{\cdot}10^{-3}$	$6.19{\cdot}10^{-3}$	$1.29{\cdot}10^{-3}$

In Table 5.6 one can see the values of the first 20 dimensionless natural frequencies β_{mn} obtained with basis $B_{5,5}$ with 1024 elements. In Figure 5.6 several vibration modes are shown. The obtained results are in good agreement with the analytical solution, given by Eq.(4.23).

Table 5.6: The first 20 vibration modes with their respective natural dimensionless frequencies.

Mode	Value β_{mn}	Mode	Value β_{mn}
1	3.196221	11	8.346606
2	4.6109	12	8.346606
3	4.6109	13	9.196883
4	5.905678	14	9.196883
5	5.905678	15	9.439499
6	6.306437	16	9.525701
7	7.143531	17	9.525701
8	7.143531	18	10.53667
9	7.799274	19	10.53667
10	7.799274	20	10.68703

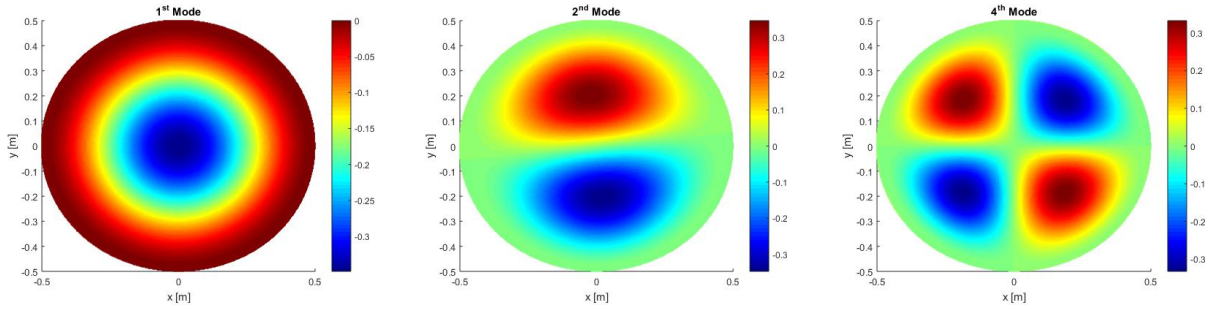

(a) 1^{st} Mode (b) 2^{nd} Mode (c) 4^{th} Mode

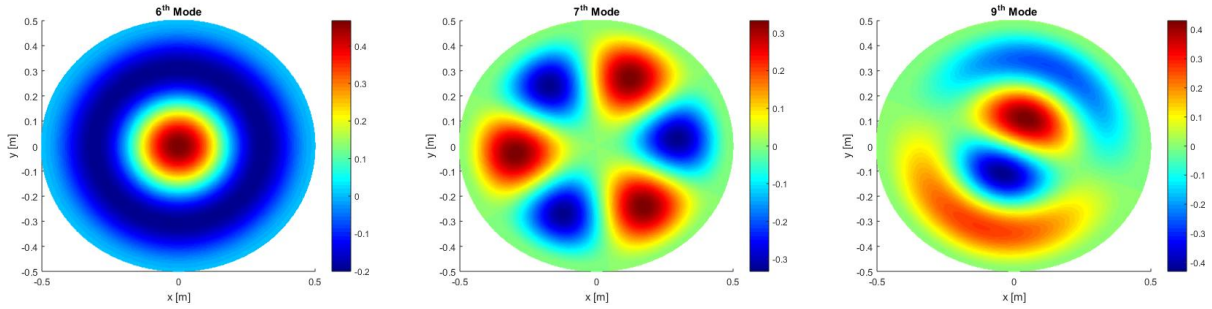

(d) 6^{th} Mode (e) 7^{th} Mode (f) 9^{th} Mode

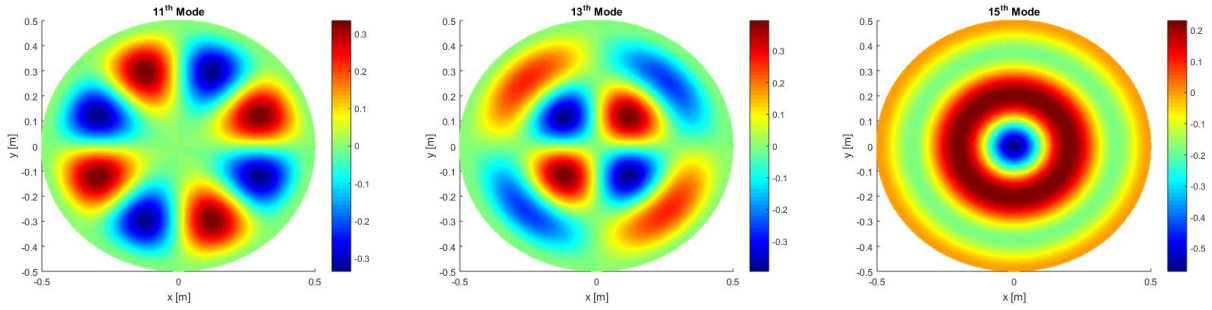

(g) 11^{th} Mode (h) 13^{th} Mode (i) 15^{th} Mode

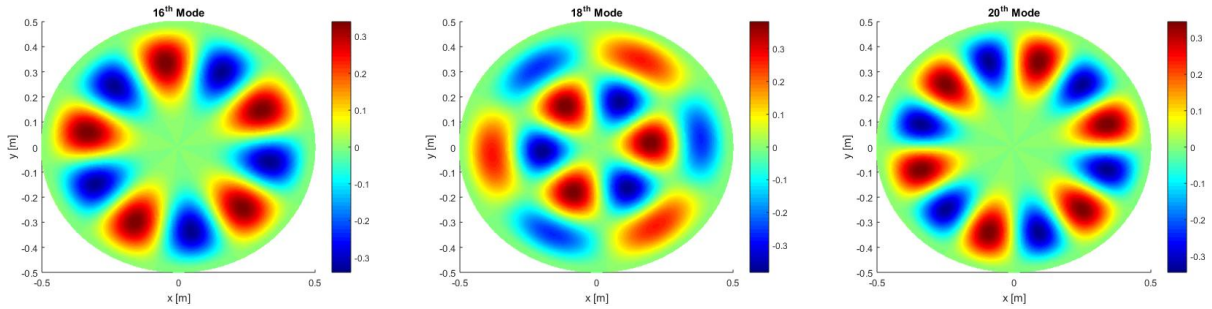

(j) 16^{th} Mode (k) 18^{th} Mode (l) 20^{th} Mode

Figure 5.6: Some of the vibration modes of a clamped circular plate.

5.2 Problem 2: Clamped Circular Plate with Two-Patch Parameterization.

5.2.1 Solution Bases for Regular Division

To study this plate in a first instance, the geometry was generated using NURBS basis functions given in Table 4.3 and Eq. (4.26) and (4.27); the corresponding result is shown in Figure 5.7. To approximate the solution, B-Splines functions were used. In order to construct the solution bases, the knot vectors used were:

$$\Sigma = \left\{0, 0, 0, \frac{1}{3}, \frac{2}{3}, 1, 1, 1\right\}, \quad \Pi = \left\{0, 0, 0, \frac{1}{4}, \frac{2}{4}, \frac{3}{4}, 1, 1, 1\right\}. \tag{5.4}$$

The B-Spline solution basis of degree $p = q = 2$ is constructed on knot vectors, see Eq. (5.4), by setting all weights to be equal to 1. The degree of the B-Splines basis is subsequently raised using the algorithm of degree elevation to $p = q = 3, 4, 5$. In what follows, the corresponding bases are denoted as $B^k_{p,q}$, where k denotes the patch number used to generate the geometry. Then the h-refinement by knot insertion is performed.

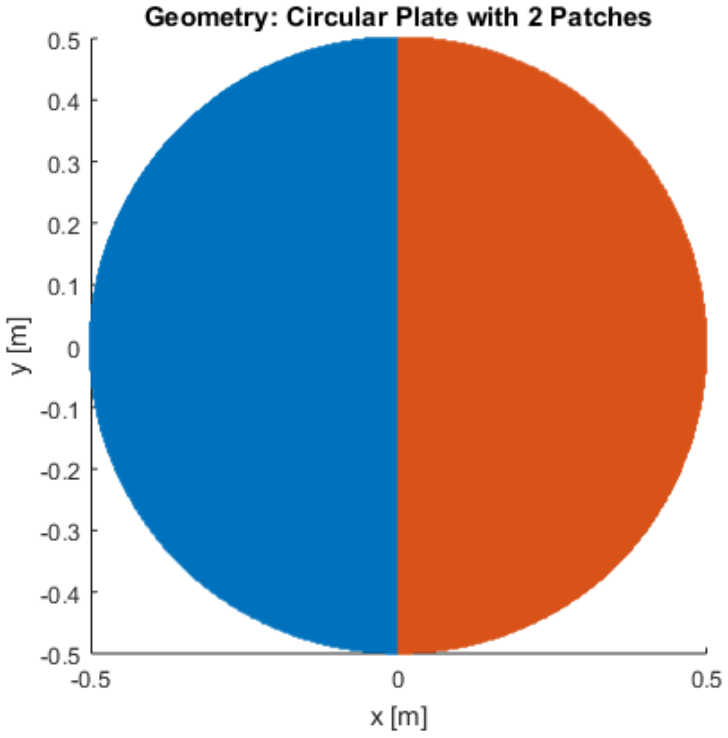

Figure 5.7: Geometry of a circular plate of radius $a = 0.5[m]$ of 2 patches generated with NURBS functions.

5.2.2 Bending Symmetric Problem for a Regular Division

For this case, in Figures 5.8 and 5.9, the deformed shape is shown, obtained both theoretically and numerically. The numerical results, shown graphically in Figure 5.9, were obtained by using basis $B^2_{5,5}$ and 1230 elements.

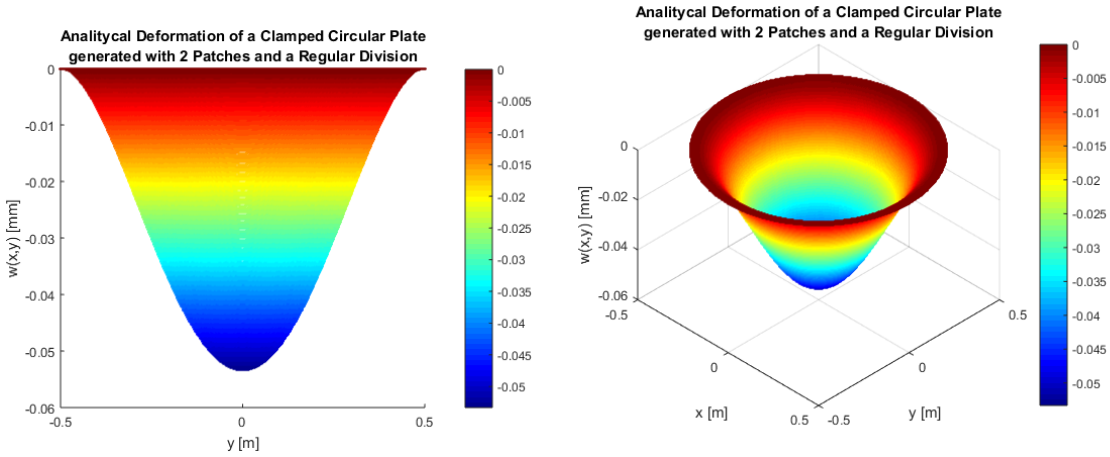

(a) Front view. (b) 3-D view.

Figure 5.8: Theoretical transverse displacement of a clamped circular plate generated with 2 patches and with a regular division.

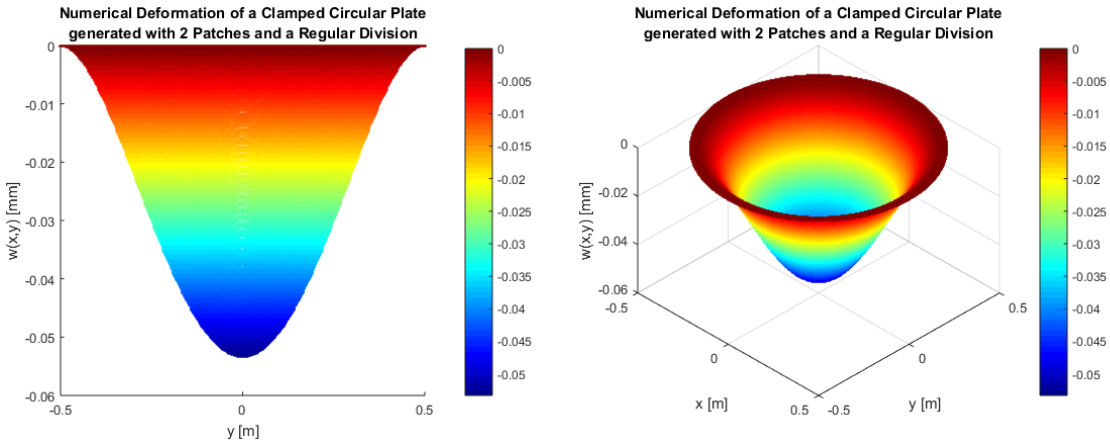

(a) Front view. (b) 3-D view.

Figure 5.9: Numerical transverse displacement of a clamped circular plate generated with 2 patches and with a regular division.

Figure 5.10 shows the comparison between the theoretical displacement and the numerical solution obtained using $B^2_{5,5}$ and 1230 elements.

Figure 5.11 shows the convergence curves obtained for the different degrees of polynomials and B-Splines basis functions for the solution approximation, namely $B^1_{2,2}$, $B^2_{2,2}$, $B^1_{3,3}$, $B^2_{3,3}$, $B^1_{4,4}$, $B^2_{4,4}$, $B^1_{5,5}$ y $B^2_{5,5}$.

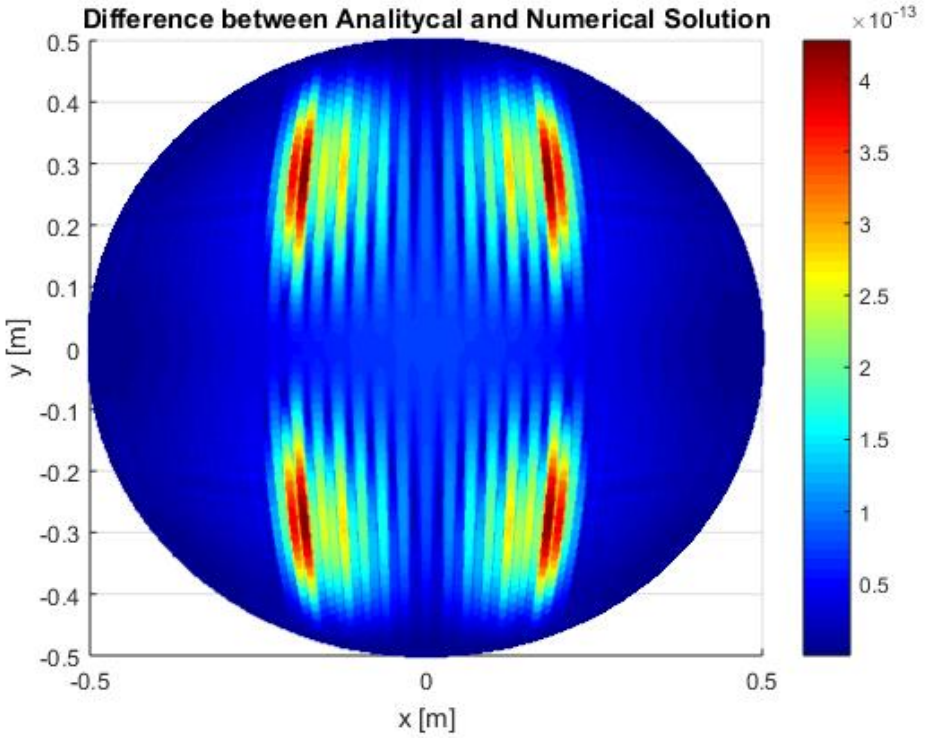

Figure 5.10: Absolute difference between the theoretical displacement and the numerical solution obtained using $B^2_{5,5}$ and 1230 elements.

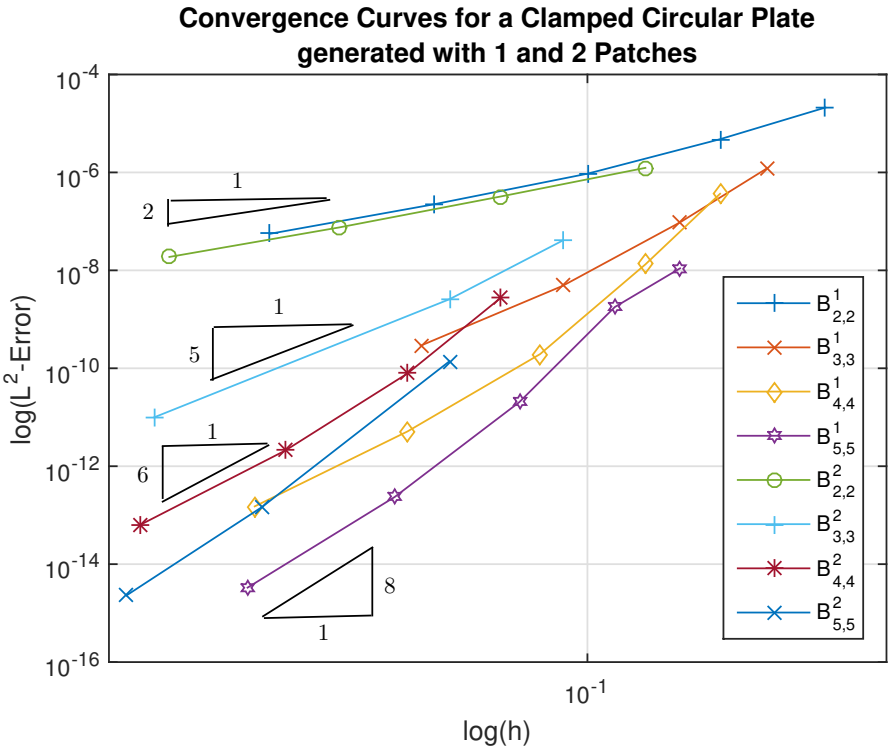

Figure 5.11: Convergence curves of the different cases studied for a clamped circular plate with 1 pacth and 2 patches regularly divided .

Table 5.7 shows the slopes for the different cases of convergence studied and presented graphically in Figure 5.11.

Table 5.7: Convergence rates for the cases studied.

(p, q)	Theory [24] [25] [26]	1 Patch	2 Patches
(2,2)	3	2.2	2.13
(3,3)	4	5.15	4.89
(4,4)	5	6	6.26
(5,5)	6	7.53	7.97

5.2.3 Solution Bases for Irregular Divisions

To study how different parameterizations may affect the results already obtained, 2 irregular ways of dividing the circle were studied: the $\succ$-shape and the $\wr$-shape. For both cases, the geometry was generated using NURBS basis functions given in Eq. (4.26) and (4.27), and in Tables 4.4 and 4.5, respectively; the corresponding result for each parameterization is shown in Figure 5.12. To approximate the solution, B-Splines functions were used. In order to construct the solution bases, the same knot vectors used in the first part of this problem section are used, i.e, see Eq. (5.4).

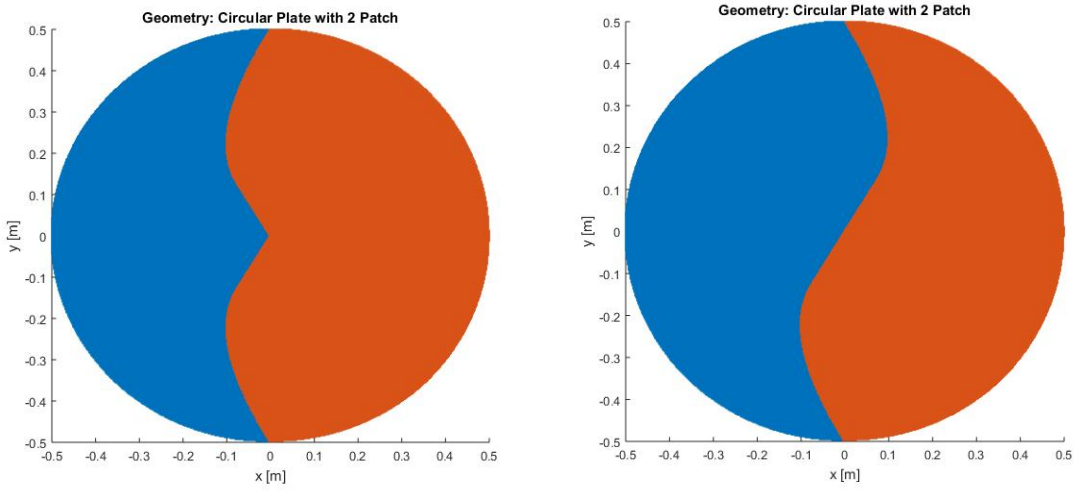

(a) $\succ$-shape parameterization. (b) $\wr$-shape parameterization.

Figure 5.12: The two parameterizations of a circle with an irregular division using NURBS functions.

The B-Spline solution basis of degree $p = q = 2$ is constructed on knot vectors, see Eq. (5.4), by setting all weights to be equal to 1. The degree of the B-Splines basis is subsequently raised using the algorithm of degree elevation to $p = q = 3, 4, 5$. In what follows, the corresponding bases are denoted as $B^S_{p,q}$, where S denotes the type of irregular parametrization used to generate the geometry: $S = SC$ corresponds to $\succ$-shape and $S = SS$ to $\wr$-shape. Then the h-refinement by knot insertion is performed.

5.2.4 Bending Symmetric for Irregular Divisions

For this case, in Figures 5.13 and 5.14, the deformed shape obtained numerically is shown. The numerical results, shown graphically in Figure 5.13 were obtained by using basis $B^{SC}_{5,5}$ and 1230 elements; while in Figure 5.14, the results were obtained using basis $B^{SS}_{5,5}$ and the same number of elements.

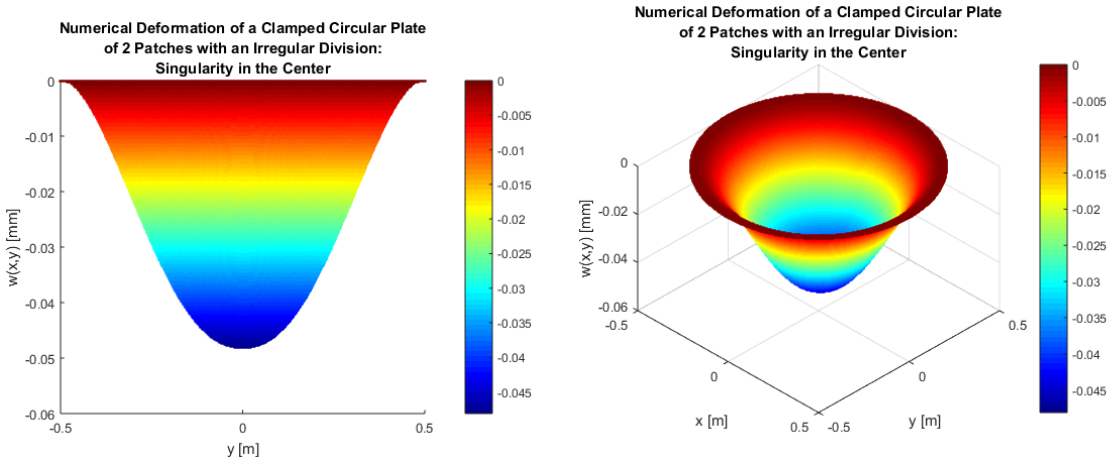

(a) Front view. (b) 3-D view.

Figure 5.13: Numerical transverse displacement of a clamped circular plate generated with $\succ$-shape parameterization.

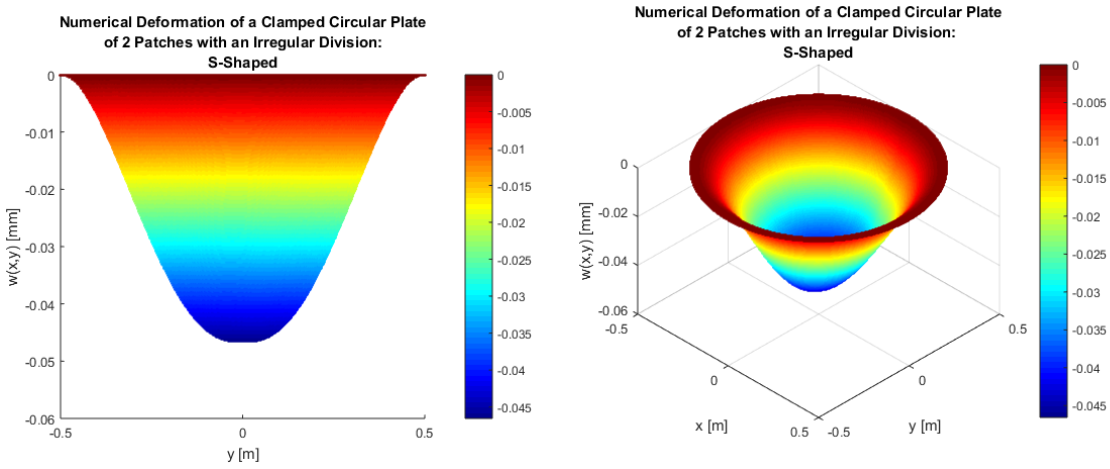

(a) Front view. (b) 3-D view.

Figure 5.14: Numerical transverse displacement of a clamped circular plate generated with $\wr$-shape parameterization.

Figure 5.15 shows the comparison between the theoretical displacement and the numerical solution for both irregular parameterizations. The numeral results were obtained using $B^{SC}_{5,5}$ and $B^{SS}_{5,5}$, for $\succ$-shape and $\wr$-shape parameterization, respectively; and 1230 elements.

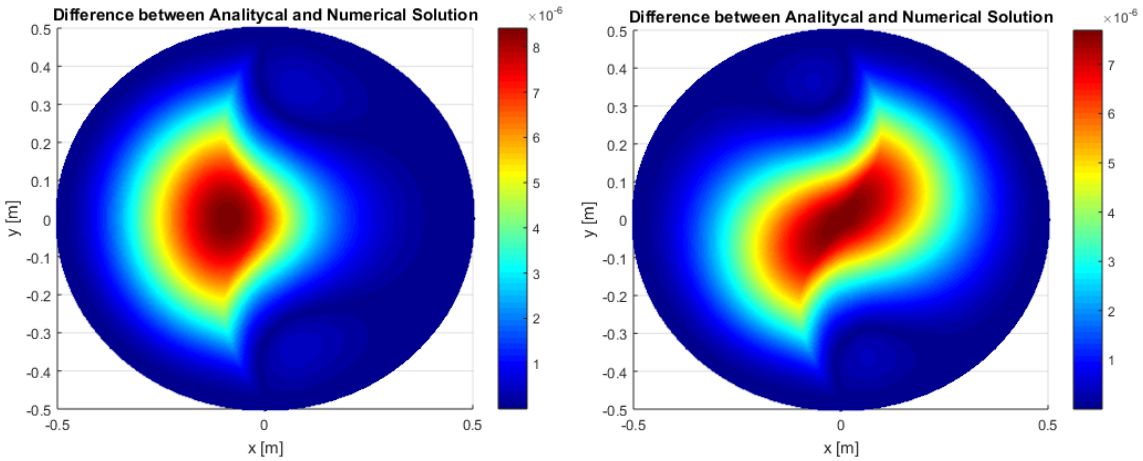

(a) $\succ$-shape parameterization. (b) $\wr$-shape parameterization.

Figure 5.15: Absolute difference between the theoretical displacement and the numerical solution obtained using $B^{SC}_{5,5}$ and $B^{SS}_{5,5}$, for $\succ$-shape and $\wr$-shape parameterization, respectively, and 1230 elements.

Figure 5.16 shows the convergence curves obtained for the different degrees of polynomials and B-Splines basis functions for the solution approximation, namely $B^{SC}_{2,2}$, $B^{SS}_{2,2}$, $B^{SC}_{3,3}$, $B^{SS}_{3,3}$, $B^{SC}_{4,4}$, $B^{SS}_{4,4}$, $B^{SC}_{5,5}$ y $B^{SS}_{5,5}$.

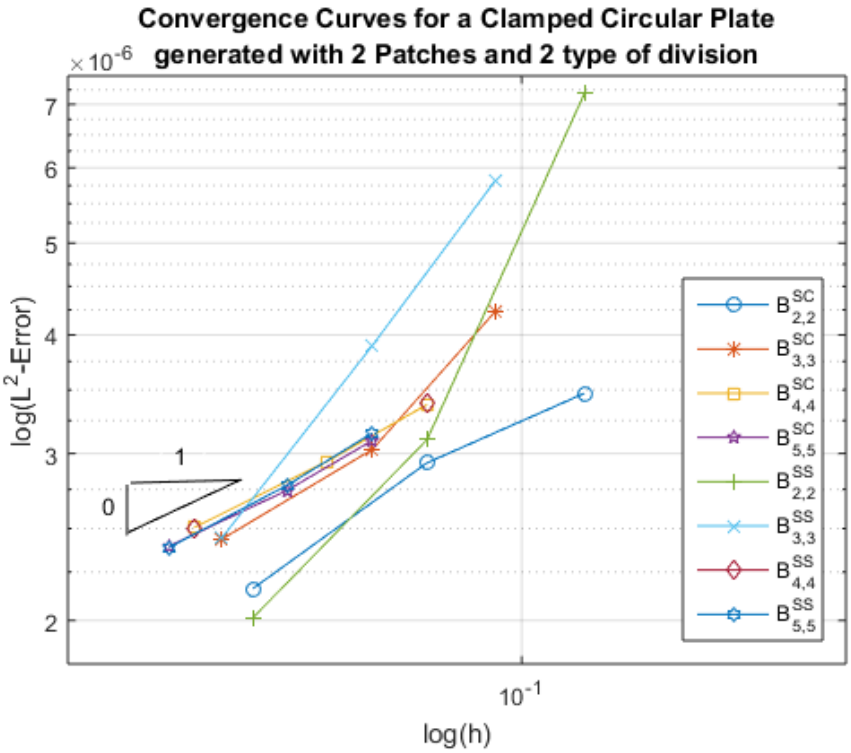

Figure 5.16: Convergence curves of the different cases studied for a clamped circular plate generated with the 2 irregular parameterizations: $\succ$-shape and $\wr$-shape.

5.3 Problem 3: Clamped Square Plate with a cut-out of Complicated Shape, composed by 8 Patches

5.3.1 Solution Bases

To study this plate, the geometry was generated using NURBS basis functions given in Table 4.8, and the corresponding result is shown in Figure 5.17. To approximate the solution, B-Splines functions were used. In order to construct the solution bases, the knot vectors used were:

$$\Sigma = \left\{0, 0, 0, \frac{1}{8}, \frac{2}{8}, \frac{3}{8}, \frac{4}{8}, \frac{5}{8}, \frac{6}{8}, \frac{7}{8}, 1, 1, 1\right\}, \quad \Pi = \{0, 0, 0, 1, 1, 1\}. \tag{5.5}$$

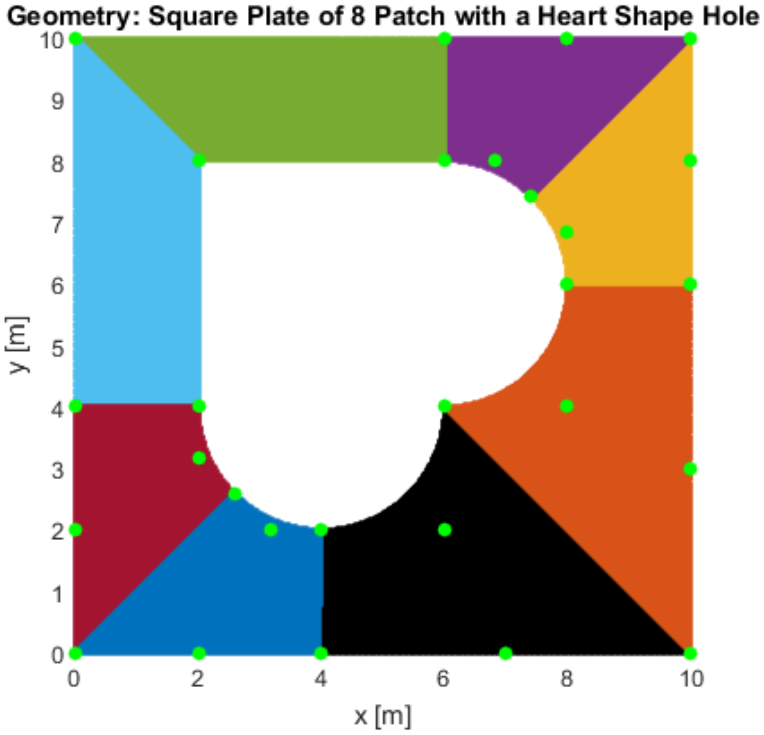

Figure 5.17: Geometry of an Square Plate with a Complicated Hole of 8 patches using NURBS functions and the control points distribution represented by green points.

The B-Spline solution basis of degree $p = q = 2$ is constructed on knot vectors, see Eq. (5.5), by setting all weights to be equal to 1. The degree of the B-Splines basis is subsequently raised using the algorithm of degree elevation to $p = q = 3, 4$. In what follows, the corresponding bases are denoted as $B_{p,q}$. Then the h-refinement by knot insertion is performed.

5.3.2 Bending Problem

For this case, in Figures 5.18 and 5.19, the deformed shape obtained numerically is shown. The numerical results, shown graphically in Figure 5.18, were obtained by using basis $B_{4,4}$ and 624 elements; while in Figure 5.19, the results were obtaining by an ANSYS simulation.

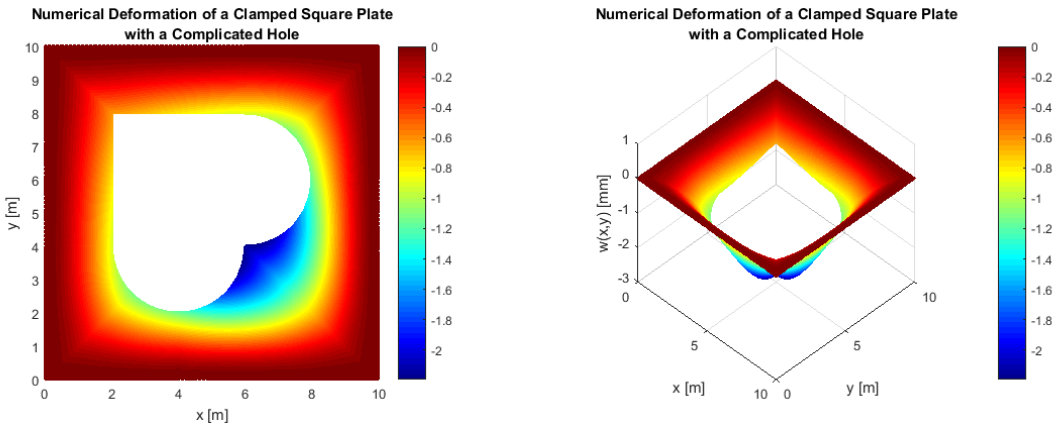

(a) Front view.

(b) 3-D view.

Figure 5.18: Numerical transverse displacement of a clamped square plate with a hole with complicated shape.

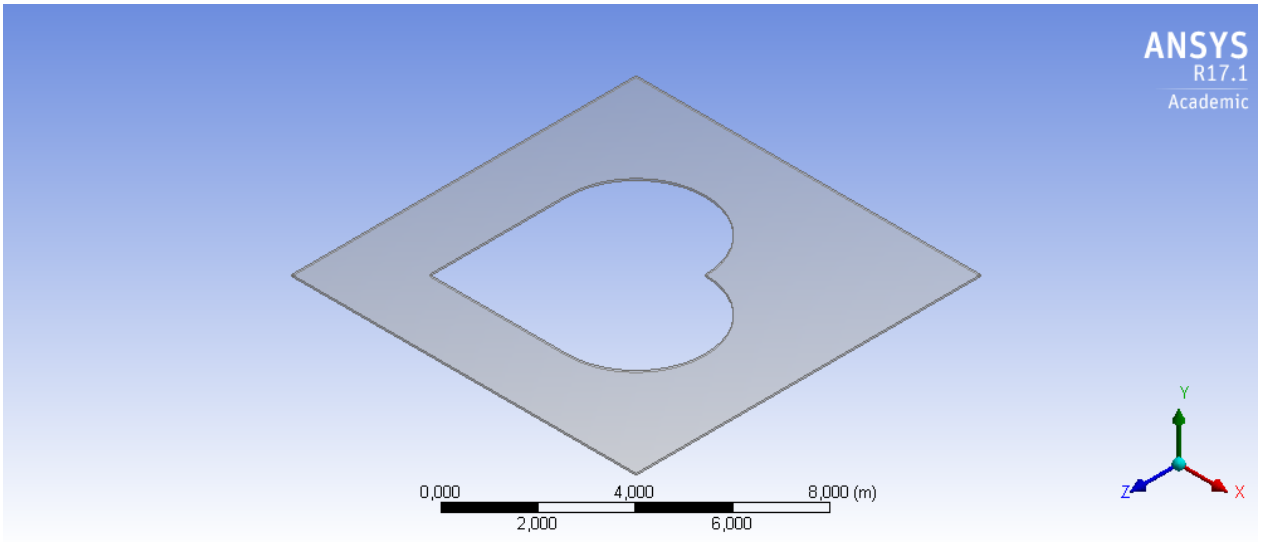

(a) Model in ANSYS of the plate.

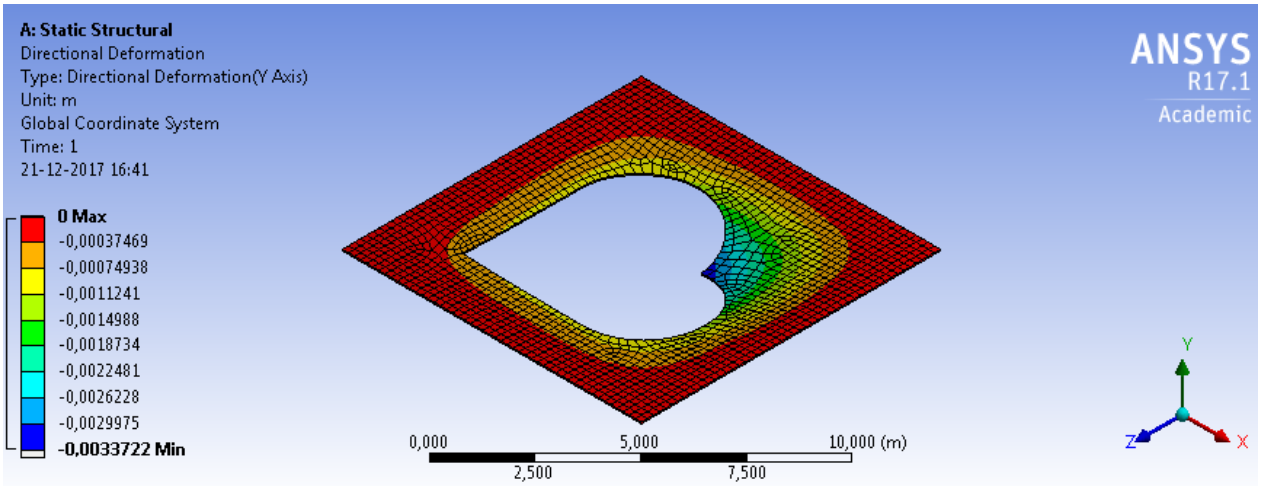

(b) Numerical transverse displacement of the plate obtained with ANSYS.

Figure 5.19: Model and transverse displacement obtained with ANSYS.

5.3.3 Free Vibrations Problem

The natural dimensionless frequencies for this case are defined as:

$$\lambda_{\mathrm{i}} = \left(w_{\mathrm{i}}^2 L^4 \frac{\rho h}{D} \right)^{1/4} \tag{5.6}$$

Table 5.8 presents the results obtained for the first 10 dimensionless natural frequencies with the present method using basis $B_{4,4}$ with 624 elements and other methods to compare the accuracy of this. The results coming from the other methods come from: Shuohui Yin et al. [22] using isogeometric approach based on the first order shear deformation plate theory (FSDT), Xinkang Li et al. [27] using IGA based on the third order shear deformation plate

theory (TSDT), X. Y. Cui et al. [28] using the radial point interpolation method with edge-based smoothing operations (ES-RPIM), Khuong D. Nguyen et al. [8] using isogeometric finite element for three-dimensional functionally graded material plate structure (3D FGM), S-FSDT based on IGA [22], Kirchhoff on the IGA [13], MKI method [29], EFG method [30] and node-based smoothing RPIM (NS-RPIM) method [28].

To compare the accuracy of the results listed in Table 5.8, the percentage difference is defined as:

$$\%_{Difference} = \left| \frac{\lambda_{\mathrm{i},GIFT} - \lambda_{\mathrm{i},M_j}}{\frac{1}{2}\left(\lambda_{\mathrm{i},GIFT} + \lambda_{\mathrm{i},M_j}\right)} \right| \cdot 100 \tag{5.7}$$

Where, $\lambda_{\mathrm{i},GIFT}$ and λ_{i,M_j} represent the i$-$th dimensionless natural frequency obtained with the GIFT method and the $j-$th method mentioned above, respectively.

In Table 5.8 one can see the values of the first 10 dimensionless natural frequencies λ_{i} obtained with basis $B_{4,4}$ with 624 elements. In Figure 5.20, the first 10 vibration modes are shown.

Table 5.8: Comparison of the dimensionless natural frequency λ_{i} of an isotropic thin square plate with a complicated shape hole and clamped in its edges.

Mode		GIFT	3D FGM based IGA [8]	Kirchhoff based IGA [13]	EPG [30]	NS-RPM [28]	ES-RPM [28]	FSDT based IGA [22]	S-FSDT based IGA [22]	TSDT based IGA [27]
1	Value	7.905	7.448	7.621	7.548	7.410	7.423	7.453	7.431	7.558
	$\%_{Difference}$	-	5.954	3.659	4.621	6.465	6.290	5.887	6.182	4.489
2	Value	9.722	9.817	9.810	10.764	9.726	9.770	9.825	9.880	10.056
	$\%_{Difference}$	-	0.973	0.902	10.173	0.042	0.493	1.054	1.613	3.378
3	Value	9.824	9.849	9.948	11.113	9.764	9.797	9.845	9.992	10.106
	$\%_{Difference}$	-	0.255	1.255	12.314	0.613	0.276	0.214	1.696	2.830
4	Value	10.901	10.952	11.135	11.328	10.964	10.927	10.964	11.077	11.191
	$\%_{Difference}$	-	0.467	2.124	3.842	0.577	0.239	0.577	1.602	2.626
5	Value	11.106	11.172	11.216	12.862	11.165	11.137	11.165	11.254	11.361
	$\%_{Difference}$	-	0.593	0.986	14.653	0.530	0.279	0.530	1.324	2.270
6	Value	12.305	12.348	12.482	13.300	12.381	12.363	12.381	12.424	12.529
	$\%_{Difference}$	-	0.349	1.429	7.772	0.616	0.471	0.616	0.963	1.804
7	Value	12.471	12.871	12.872	14.168	12.953	12.822	12.953	12.862	13.110
	$\%_{Difference}$	-	3.157	3.165	12.741	3.792	2.776	3.792	3.087	4.996
8	Value	13.413	13.505	13.650	15.369	13.721	13.428	13.721	13.678	13.763
	$\%_{Difference}$	-	0.684	1.752	13.592	2.271	0.112	2.271	1.957	2.576
9	Value	14.510	14.457	14.676	16.205	14.511	14.508	14.511	14.227	14.645
	$\%_{Difference}$	-	0.366	1.138	11.037	0.007	0.014	0.007	1.970	0.927
10	Value	14.819	14.730	14.738	17.137	14.792	14.789	14.792	14.613	14.913
	$\%_{Difference}$	-	0.603	0.549	14.508	0.183	0.203	0.183	1.400	0.633

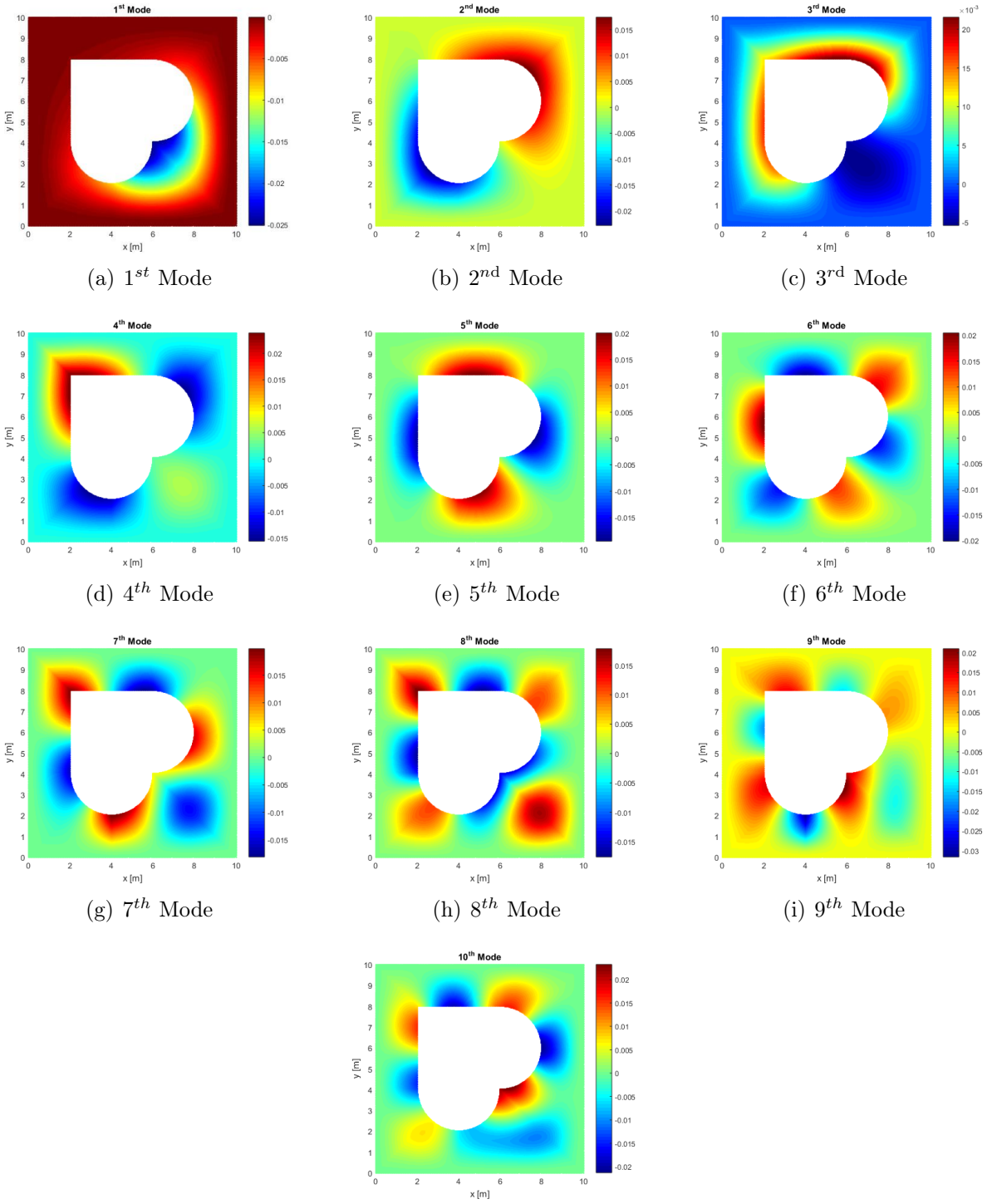

(a) 1^{st} Mode (b) 2^{nd} Mode (c) 3^{rd} Mode

(d) 4^{th} Mode (e) 5^{th} Mode (f) 6^{th} Mode

(g) 7^{th} Mode (h) 8^{th} Mode (i) 9^{th} Mode

(j) 10^{th} Mode

Figure 5.20: First 10 modes of vibration of a clamped square plate with a hole of complicated shape.

Chapter 6

Analysis and Discussion

In this chapter, the results obtained for three problems of bending and vibration of the KLPT plates will be analyzed and discussed.

6.1 Problem 1: Clamped Circular Plate with 1 Patch

In the first problem, symmetric bending and free vibration problems were studied for a clamped circular plate, whose geometry was generated with 1 patch.

From Figures 5.2 and 5.3, it can be noted that the numerical results obtained with the GIFT method for the problem of bending of a circular plate clamped at the edge are quite similar to those predicted by the theory. Inclusively, in Figure 5.4 it can be seen that the absolute difference between the numerical values w_N and analytical w_A, when using NURBS functions and polynomials of degree 5 with $h-$refinement, are of the order of $|w_N - w_A| \approx 10^{-15}[m]$.

From the convergence curves plotted in Figure 5.5, it can be seen that the finer the mesh or higher the order of the basis functions (NURBS or B-Splines), more accurate the results are, as expected. From Figure 5.5 and Table 5.1, it can be seen that for the same polynomial order $p = q = 2, 3, 4, 5$ the convergence results obtained with NURBS bases are quasi identical to the results, obtained by the B-Splines.

As discussed in [24], [25] and [26], the theoretical convergence rate for this type of problem is $p + 1$. Comparing the convergence rates obtained theoretically and numerically for each degree of polynomial $p = q$, using both NURBS and B-Splines functions, and presented in Table 5.1; it can be seen that the numerical value of the slope for the case $p = q = 2$ is less than the theoretical and for the rest of the cases studied, they are larger, which contradicts what was expected by the theory.

But this error with the theory is due to the computational limitations of this thesis work and not to errors in the implementation of the GIFT method, because as can be seen in

Figure 5.5, the convergence curves show a monotonously decreasing behavior as the size of the element h decreases, where the convergence rate also decreases with this and tends to the theoretical values expected, but given the computational limitations, the results for finer meshes that show the rate can not be obtained to which, for each degree of polynomial, the curve presents an asymptotic behavior.

From the results on the dimensionless natural frequencies β_{mn} tabulated in 5.2- 5.5, we can see that when using polynomials of grade $p = q = 2$ with $h-$refinement, percentage errors are obtained within the range $[10^{-1}, 1]$, while that by using polynomials of degree $p = q = 5$ with $h-$refinement, the percentage error decreases and is in the range $[10^{-5}, 10^{-3}]$. In addition, it can be noted that the results obtained using NURBS and B-Splines for the same case, are similar in magnitude. These results coincide with what was expected by increasing the degree of the polynomial of the basis functions and refining the mesh.

6.2 Problem 2: Clamped Circular Plate with 2 Patches

In the second problem, only the symmetrical bending was studied for circular plate, whose geometry was generated with 2 patches of 3 different forms, which can be classified as regular and irregular.

In the Figures 5.7 and 5.12, one can see the 3 different ways in which the geometry of the circular plate was generated. Out of these, Figure 5.7 shows a division of the regular type, while the Figure 5.12 are of the irregular type.

Analyzing the problem of symmetrical bending for the case in which the geometry is generated with a regular division of the 2 patches, it can be observed from the Figures 5.8 and 5.9 that the deflections obtained numerically with the GIFT are quite similar to those predicted by the theory. Additionally, in Figure 5.10 it can be seen that the absolute difference between the numerical values w_N and analytical w_A, when using B-Splines functions and polynomials of degree 5 with $h-$refinement, are of the order of $|w_N - w_A| \approx 10^{-13}[m]$.

From Figure 5.11 and Table 5.7, we can see that the convergence curves and the slopes corresponding to the same solution bases of $p = q = 2, 3, 4, 5$ but different (one-patch and two-patch) geometry parameterizations, are quite similar. The overall error for the one-patch geometry is smaller than for the two-patch parameterization, but this slight difference in the accuracy comes with the significant advantage, that the original smooth two-patch parameterization can be used directly, without any coupling between patches, as well as without elevating its degree.

As discussed in the work of [24], [25] and [26]; the theoretical convergence ratio for this type of problem is $p+1$. Comparing the convergence rates obtained theoretically and numerically for each degree of polynomial $p = q$, using B-Splines functions, and presented in Table 5.7; it can be seen that the numerical value of the slope for the case $p = q = 2$ is less than the theoretical and for the rest of the cases studied, they are larger, which contradicts what was expected by the theory.

Similar to the analysis performed in Problem 1, this error with the theory is due to the computational limitations of this thesis work and not to errors in the implementation of the GIFT method, because as can be seen in Figure 5.11, the convergence curves show a monotonously decreasing behavior as the size of the element h decreases, where the convergence rate also decreases with this and tends to the theoretical values expected, but given the computational limitations, the results for finer meshes that show the rate can not be obtained to which, for each degree of polynomial, the curve presents an asymptotic behavior.

For the case in which the problem of bending of the circular plate generated with the 2 irregular parameterizations, shown in Figure 5.12 is studied, it can be seen in Figures 5.13 and 5.14 that the maximum deflection reached by both has a value of $w_{max} \approx -0.048[mm]$, which represents approximately an 10% of error compared to the expected theoretical value given by the Eq. (5.2). The latter can also be observed in Figures 5.15a and 5.15b, the absolute differences between the numerical values w_N and analytical w_A for both parameterizations: $\succ$-shape and $\wr$-shape, respectively; when using B-Splines functions and polynomials of degree 5 with $h-$refinement for both cases, are of the order of $|w_N - w_A| \approx 10^{-6}[m]$.

Additionally, in Figures 5.15a and 5.15b, you can observer that the maximum errors for both parameterizations, $\succ$-shape and $\wr$-shape, are concentrated in the irregular joint of the patches.

In Figure 5.16, the convergence curves for both irregular parameterizations of the circle tend to a constant value if we keep refining the solution field, which indicates that the GIFT method does not allow obtaining an accurate solution for this type of geometry parameterization. This zero convergence rate for each of the cases studied is due to the repetition of control points in the center of the circle to generate $\succ$-shape and $\wr$-shape, and as can be observed in the physical meshes generated in Figures 4.4 and 4.5, distortions of the mesh and discontinuities of the basis functions occur at the border joining both patches; which does not allow to obtain an accurate solution for this problem. However, note, that such irregular parameterizations present the same difficulty for a standard IGA and are avoided in practice.

6.3 Problem 3: Clamped Square Plate with a cut-out of Complicated Shape, composed by 8 Patches

In the last problem of this work, symmetric bending and free vibration problems were studied for a clamped square plate with a complicated shape hole, whose geometry was generated with 8 patches, as shown in Figure 5.17.

Comparing the results obtained for the bending problem of this plate with the GIFT method and the ANSYS simulation, results that are presented graphically in Figures 5.18 and 5.19, it can be seen that for the maximum displacement of the plate there is a percentage difference between the both methods of approximately 33 %. This may be due to the low continuity of the geometry parameterization across the boundary between the patches, analogously to the situation with the irregular two-patch parameterizations of the circle in Problem 2.

In Table 5.20, the numerical values of the dimensionless natural frequencies λ_i obtained by the GIFT method are compared with the results available in the literature and obtained by other methods. It can be seen that the GIFT yields the results which are very similar to those obtained by the others authors.

6.4 Discussion

Based on the results obtained in this work, the following can be observed:

- GIFT, in general, can be used for problems of bending and vibration of Kirchoff-Love plates, described by PDEs of 4th order.
- The numerical results obtained for all cases with smooth geometry parameterization are accurate and consistent with the reference solutions.
- For other cases, where the geometry parameterizations have low continuity, the method yields lower convergence rates and the error is accumulated around irregular points, analogously to the situations commonly observed in the standard IGA.
- The difference between the results, obtained with the NURBS bases (for the solution approximation) derived from the original geometry parameterizations and the results obtained with the B-Splines bases are quasi identical (comparing the NURBS and B-Splines bases of the same degree). Note, that in the latter case, during the solution refinement process, there is no need to refine the weights and therefore this approach has a potential to provide significant computational savings, when applied to large scale problems.
- It is demonstrated that the multi-patch geometries can be paired with one-patch solution basis, given by B-Splines. In this cases, no additional coupling is required between the geometry patches. Based on the obtained results, the smooth geometry parameterization provides the most accurate results. However, the use of geometry parameterization with low continuity is still possible and yields solutions of acceptable precision.

Conclusions

In this work, the application of the new method, proposed in [3], to problems of bending and vibration of Kirchhof-Love plates, has been demonstrated. The performance of the method was studied in three different problems, which take into account various one and multi-patch geometry parameterizations and the solution field bases. The obtained results are compared with the reference solutions. The limitations of the method are also discussed.

The GIFT method, as already presented in this thesis work, presents a series of characteristics that surpass it by traditional methods of resolution, such as IGA and FEM. This allows it to be shown as a feasible alternative to solve various problems present in current engineering, such as: failure analysis of equipment components, fracture study and propagation of cracks, heat transfer, structural analysis, among others; and all this thanks to the fact that the method employs resources efficiently, it presents greater flexibility and adaptability that allow it to work with more complex geometries without losing accuracy of the solution.

Given the incipient of the method, the future work has to develop consists in showing the applicability of the method to solve other physical phenomena and engineering problems, also to further develop the GIFT to increase the accuracy of the results obtained for problems where the geometry of the object presents significant discontinuities.

Bibliography

[1] Cottrell, T. J. R. Hughes, Y. Bazilevs, and W. I. O. service, "Isogeometric analysis toward integration of CAD and FEA," 2009.

[2] J. Kiendl, K.-U. Bletzinger, J. Linhard, and R. Wüchner, "Isogeometric shell analysis with kirchhoff–love elements," *Computer Methods in Applied Mechanics and Engineering*, vol. 198, no. 49, pp. 3902–3914, 2009.

[3] E. Atroshchenko, G. Xu, S. Tomar, and S. Bordas, "Weakening the tight coupling between geometry and simulation in isogeometric analysis: from sub-and super-geometric analysis to geometry independent field approximation (gift)," *arXiv preprint arXiv:1706.06371*, 2017.

[4] K.-J. Bathe, *Finite element procedures*. Klaus-Jurgen Bathe, 2006.

[5] J. N. Reddy, *An introduction to the finite element method*, vol. 2. McGraw-Hill New York, 1993.

[6] T. J. Hughes, J. A. Cottrell, and Y. Bazilevs, "Isogeometric analysis: Cad, finite elements, nurbs, exact geometry and mesh refinement," *Computer methods in applied mechanics and engineering*, vol. 194, no. 39, pp. 4135–4195, 2005.

[7] L. Coradello, "Implementation of a high-order kirchhoff-love shell: a comparison of iga and p-fem," 2015.

[8] K. D. Nguyen and H. Nguyen-Xuan, "An isogeometric finite element approach for three-dimensional static and dynamic analysis of functionally graded material plate structures," *Composite Structures*, vol. 132, pp. 423–439, 2015.

[9] O. Bauchau and J. Craig, "Kirchhoff plate theory," in *Structural analysis*, pp. 819–914, Springer, 2009.

[10] A. A. R. Mohammad Amin Rashidifar, "Vibrations analysis of circular plate with piezoelectric actuator using thin plate theory and bessel function," *American Journal of Engineering, Technology and Society*, vol. 2, no. 6, pp. 140–156, 2015.

[11] A. W. Leissa, "Vibration of plates," tech. rep., OHIO STATE UNIV COLUMBUS, 1969.

[12] M. L. Bittencourt, *Computational Solid Mechanics: Variational Formulation and High*

Order Approximation. CRC Press, 2014.

[13] S. Shojaee, E. Izadpanah, N. Valizadeh, and J. Kiendl, "Free vibration analysis of thin plates by using a nurbs-based isogeometric approach," *Finite Elements in Analysis and Design*, vol. 61, pp. 23–34, 2012.

[14] S. S. Rao, *Vibration of continuous systems*. John Wiley & Sons, 2007.

[15] R. G. Anderson, B. Irons, and O. Zienkiewicz, "Vibration and stability of plates using finite elements," *International Journal of solids and Structures*, vol. 4, no. 10, pp. 1031–1055, 1968.

[16] L. B. da Veiga, A. Buffa, C. Lovadina, M. Martinelli, and G. Sangalli, "An isogeometric method for the reissner–mindlin plate bending problem," *Computer Methods in Applied Mechanics and Engineering*, vol. 209, pp. 45–53, 2012.

[17] C. H. Thai, A. Ferreira, S. P. A. Bordas, T. Rabczuk, and H. Nguyen-Xuan, "Isogeometric analysis of laminated composite and sandwich plates using a new inverse trigonometric shear deformation theory," *European Journal of Mechanics-A/Solids*, vol. 43, pp. 89–108, 2014.

[18] S. Natarajan, H. Nguyen-Xuan, A. Ferreira, and E. Carrera, "Static bending and free vibration of cross ply laminated composite plates using nurbs based finite element method and unified formulation," *arXiv preprint arXiv:1312.4032*, 2013.

[19] X. Li, J. Zhang, and Y. Zheng, "Nurbs-based isogeometric analysis of beams and plates using high order shear deformation theory," *Mathematical Problems in Engineering*, vol. 2013, 2013.

[20] P. Gujar and K. Ladhane, "Bending analysis of simply supported and clamped circular plate," *International Journal of Civil Engineering*, vol. 2, no. 5, pp. 69–75, 2015.

[21] A. Tixier, S. Herbette, S. Jansen, M. Capron, P. Tordjeman, H. Cochard, and E. Badel, "Modelling the mechanical behaviour of pit membranes in bordered pits with respect to cavitation resistance in angiosperms," *Annals of botany*, vol. 114, no. 2, pp. 325–334, 2014.

[22] S. Yin, J. S. Hale, T. Yu, T. Q. Bui, and S. P. Bordas, "Isogeometric locking-free plate element: a simple first order shear deformation theory for functionally graded plates," *Composite Structures*, vol. 118, pp. 121–138, 2014.

[23] S. Shojaee, N. Valizadeh, E. Izadpanah, T. Bui, and T.-V. Vu, "Free vibration and buckling analysis of laminated composite plates using the nurbs-based isogeometric finite element method," *Composite Structures*, vol. 94, no. 5, pp. 1677–1693, 2012.

[24] F. Bonaldi, D. A. Di Pietro, G. Geymonat, and F. Krasucki, "A hybrid high-order method for kirchhoff-love plate bending problems," *arXiv preprint arXiv:1706.06781*, 2017.

[25] H. Santos, J. Evans, and T. Hughes, "Generalization of the twist-kirchhoff theory of plate elements to arbitrary quadrilaterals and assessment of convergence," *Computer Methods in Applied Mechanics and Engineering*, vol. 209, pp. 101–114, 2012.

[26] S. Mohammadi, N. Valizadeh, S. Ghorashi, S. Shojaee, and H. Ghasemzadeh, "Analysis of thin plates by a combination of isogeometric analysis and the lagrange multiplier approach," *Computational Methods in Civil Engineering*, vol. 3, no. 2, pp. 47–66, 2012.

[27] X. Li, J. Zhang, and Y. Zheng, "Static and free vibration analysis of laminated composite plates using isogeometric approach based on the third order shear deformation theory," *Advances in Mechanical Engineering*, vol. 6, p. 232019, 2014.

[28] X. Cui, G. Liu, G. Li, and G. Zhang, "A thin plate formulation without rotation dofs based on the radial point interpolation method and triangular cells," *International journal for numerical methods in engineering*, vol. 85, no. 8, pp. 958–986, 2011.

[29] T. Q. Bui and M. N. Nguyen, "A moving kriging interpolation-based meshfree method for free vibration analysis of kirchhoff plates," *Computers & structures*, vol. 89, no. 3, pp. 380–394, 2011.

[30] G. Liu and X. Chen, "A mesh-free method for static and free vibration analyses of thin plates of complicated shape," *Journal of sound and vibration*, vol. 241, no. 5, pp. 839–855, 2001.